

# Dry Cutting Experiments Database Ti6Al4V and Ck45

Hagen Klippel\*, Hagen Klippel, Stefan Süssmaier, Michal Kuffa, Konrad Wegener

*Institute of Machine Tools and Manufacturing (IWF), Department of Mechanical and Process Engineering,  
ETH Zürich, Leonhardstrasse 21, 8092 Zürich, Switzerland*

---

## Abstract

The numerical simulation of metal cutting processes requires material data for constitutive equations, which cannot be obtained with standard material testing procedures. Instead, inverse identifications of material parameters within numerical simulation models of the cutting experiment itself are necessary. The intention of the present report is the provision of results of a large scale experimental study of dry orthogonal cutting experiments of Ti6Al4V (3.7165 Grade 5) and Ck45 (AISI 1045) along with their documentation and interpretation. The process forces are evaluated and each cutting insert geometry has been measured prior to the experiments to determine the cutting edge radii for each experiment. The resulting chip forms are analysed and the averaged chip thicknesses are determined. A material characterization is performed, which includes microstructural investigations on the raw materials and is reported together with tensile test results. The assembled data set can be used for parameter identification when the experimental conditions are reproduced in numerical simulations. The cutting test results are finally used to derive coefficients for Kienzle's force model. The data is stored in the [pCloud](#) and contains process force measurement data, cutting edge radii scans, pictures of chip geometries and etched chips.

*Keywords:*

Material Characterization, Metal Cutting, Orthogonal Cutting, Dry Cutting, Ck45, AISI 1045, Ti6Al4V, Process Forces, Cutter Geometry, Chip Shape, Kienzle Coefficients

---

## 1. Introduction

The metal cutting process is characterized by harsh conditions, which comprise large plastic strains up to 700%, strain rates up to  $10^6 s^{-1}$  and temperatures ranging from  $500^\circ C$  to  $1400^\circ C$ , according to [2]. In the numerical simulation of such processes material parameters for constitutive models are required, but these conditions cannot be reproduced in neither simple (direct) experiments nor in experiments combining these effects. Instead, material parameters need to be deduced from an inverse identification, where the cutting test itself serves as a material test, as for example shown in [13, 17, 35].

Constitutive model constants taken from literature, e.g. for Ti6Al4V [10], show large variations and so do the simulation results. Raw materials specified by the respective norms,

---

*Email address:* [klippel@iwf.mavt.ethz.ch](mailto:klippel@iwf.mavt.ethz.ch) (Hagen Klippel\*)

when sourced from different suppliers and charges, shows slight variations in the chemical composition within the tolerance bands and may have undergone different manufacturing steps (drawing, rolling, forging) and heat treatments, which finally leads to a wide scatter of thermo-mechanical behaviour [14, 36]. These initial conditions of the materials are often not clear, which makes it difficult to select a suitable constitutive model parameter set from literature for the numerical simulation of documented experiments, for example in [9, 39].

Ck45 is a perlitic-ferritic steel which is easy to machine and widely used in mechanical engineering applications, e.g. for crankshafts, bolts, gears and bearings [28]. The material exhibits dynamic strain aging at elevated temperatures leading to increased yield stresses depending on plastic strain rate and temperature and thus can affect the chip formation and process forces as highlighted in [4, 5, 27].

Titanium alloys are of great industrial interest [29] and find wide use in biotechnical applications due to their biocompatibility [12] and are also popular in aeronautics [30] due to their low density and high strength. The most widely used titanium alloy is Ti6Al4V which however is considered difficult to machine because the material removal rate is low if the tool wear is to be low, since the considerable high-temperature strength inhibits temperature-induced softening during the separation process, leading to high thermal and mechanical stress in the tool [15, 31, 41].

The aim of the present publication is the documentation of a large scale testing program of (AISI 1045) and Ti6Al4V (3.7165, Grade 5) using dry quasi-orthogonal cutting experiments. The cutting tests are performed in a wide range of feed rates ( $f = 0.01..0.4mm/rev$ ) and cutting speeds ( $v_c = 10..500m/min$ ). Prior to the cutting experiments the raw materials are examined: hardness tests, as well as microstructural analyses by means of investigating etched samples and electron backscatter diffraction (EBSD) analyses are conducted to detect any irregularities, e.g. preferential grain orientations or material anisotropies, that may be caused by the manufacturing process. Tensile tests are carried out on test specimens of these materials and material parameter for quasi-stationary conditions together with the rate dependency at low strain rates, are documented.

In the orthogonal cutting tests neither lubrication nor cooling have been used. Each cutting test was performed with an unused cutting edge to minimize possible wear effects on the process. All cutting edges were measured using 3D metrology before the cutting tests to determine the cutting edge radii in the unworn state. This is necessary because the cutting edge radii can have a significant influence the process forces [1, 38, 39]. The measured process forces, chip shapes, average chip thicknesses, chip microstructures, apparent friction coefficients according to Merchant [25] and where applicable built-up edge formations and tempering colors are documented. The measured process forces are used to derive Kienzle coefficients for both materials over a large range of cutting speeds.

## 2. Material Specification

Raw materials of Ck45 and Ti6Al4V are used in cylindrical form with a diameter of  $\approx 80$  mm and a height of 90 mm. All cylinders are from the same batch of the respective material.

## 2.1. Delivery Condition of the Materials

Ti6Al4V is an alloy containing 6% (weight) Aluminium and 4% (weight) of Vanadium and consists of two phases:  $\alpha$ -phase and  $\beta$ -phase. The  $\alpha$ -phase is stabilized by aluminium and has a hcp-structure, while the  $\beta$ -phase is stabilized by vanadium, consisting of a bcc-lattice [3]. This batch of material was produced using the triple Vacuum Arc Remelting (VAR) method. After production a heat treatment at  $750^{\circ}\text{C}$  for 90 min was performed followed by air cooling. The chemical composition as specified from the supplier is given in table 1 and the tensile properties (minimum values) in table 2.

The material batch of Ck45 (C45E) was produced in an electric shaft furnace and afterwards rolled into cylindrical form. The chemical composition as specified by the supplier is shown in table 1, the tensile properties of the materials in table 2. A Jominy-test was performed by the supplier and the results are shown in table 3. The material exhibits a high hardenability at the outer surface where the hardness is up to 59 HRC which indicates a martensitic microstructure and decreases to 19 HRC with increasing distance from the surface, indicating a ferritic-perlitic microstructure.

Material	Fe	C	N	H	O	Y	Al	V	Ti	Mn	Si	P	S	Cr	Ni	Mo	Cu	Sn	Nb	B	Residuals each	total	
Ti6Al4V	0.111	0.025	0.020	0.003	0.15	<0.005	6.12	4.11	Balance	-	-	-	-	-	-	-	-	-	-	-	-	<0.1	<0.4
Ck45	Balance	0.445	-	-	-	-	0.01	0.002	0.01	0.76	0.24	0.018	0.02	0.18	0.05	0.01	0.15	0.006	0.001	0.000	-	-	-

Table 1: Ti6Al4V and Ck45: Supplier information on the chemical composition of this material batch.

Material	Tensile strength [MPa]	Yield strength (0,2% offset) [MPa]	Elongation at break [%]	Reduction of area [%]	Hardness test [HRC]
Ti6Al4V	952	869	16.5 ( $4 \cdot D$ , [34])	39	30.0
Ck45	671	420	22.2 ( $A_5$ , [7])		

Table 2: Ti6Al4V and Ck45: Supplier information on tensile test results of the respective material batch.

[mm]	1	2	3	4	5	6	7	8	9	10	11	13	15	20	25	30
HRC	59	57	54	46	37	34	30	29	28	27	26	25	24	23	21	19

Table 3: Ck45: supplier information on Jominy test results of this material batch.

## 2.2. Sample Preparation

Deep bores are inserted to the raw cylinders using EDM drilling. A smaller cylinder of 60 mm diameter is cut out via wire EDM and used to manufacture the test specimens for tensile testing, see chapter 2.5. The outer cylinders are used for orthogonal cutting experiments. A disk with a height of  $h_{disk} = 10\text{mm}$  is sliced off of one cylinder of each material using wire EDM and used to determine the radial hardness profile. The disks are ground and polished prior to the hardness measurements. After the hardness measurements, the same disks are used to prepare etched samples from the top and side surface for microstructural investigations and EBSD analyses. An overview of the material usage is shown in Figure 1.

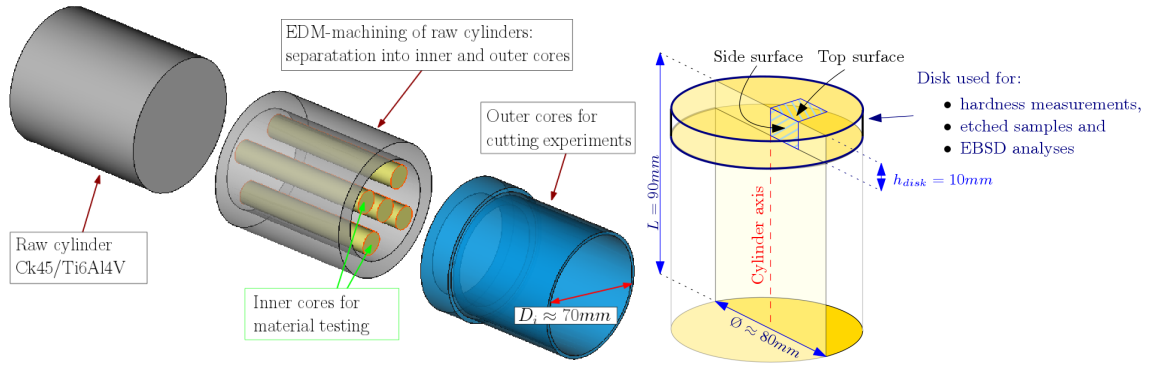


Figure 1: Left: raw material usage for material tests and orthogonal cutting tests. Right: sample orientations for hardness measurements, etched samples and EBSD analysis with surface denominations.

### 2.3. Vickers Hardness Measurement

Vickers hardness measurements HV10 are conducted for Ck45 and Ti6Al4V. The measurements are performed on the top faces along four directions of the samples where in one direction a 1 mm stepping and in the others a 2 mm stepping was used. The hardness measurement directions and both disks are shown in figure 2. The results of the hardness measurement are shown in Figure 3 where the Ck45 shows a hardness reduction at the disk center within a radius of around 6mm. Towards the outer radius the hardness is constant except for the very last measurement point in direction 2 which shows a slight drop in hardness. The hardness distribution of the Ti6Al4V sample is almost constant in all directions and radial positions with the exception of some spots.

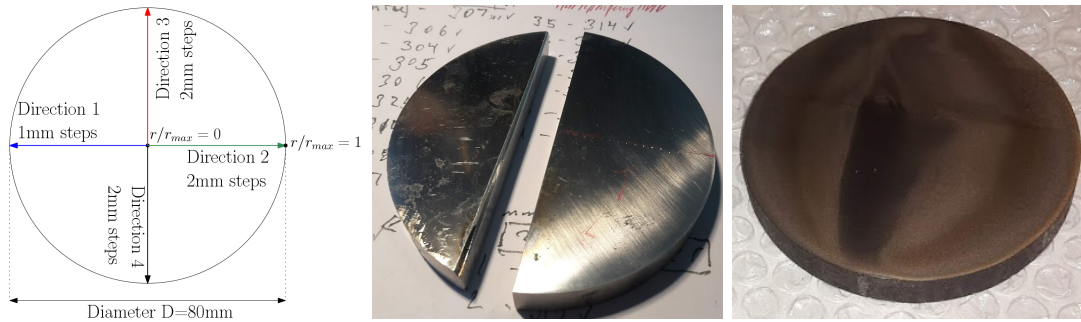


Figure 2: Hardness measurement directions (left), Ti6Al4V disk (middle) and Ck45 (right) disks from cylinders used for the hardness measurements. The Ck45 disk is shown here before grinding, polishing and hardness measurements while the Ti6Al4V is already cut in half for microstructural investigations with the right half showing imprints from the hardness measurements (2mm stepping) along the slightly visible red line.

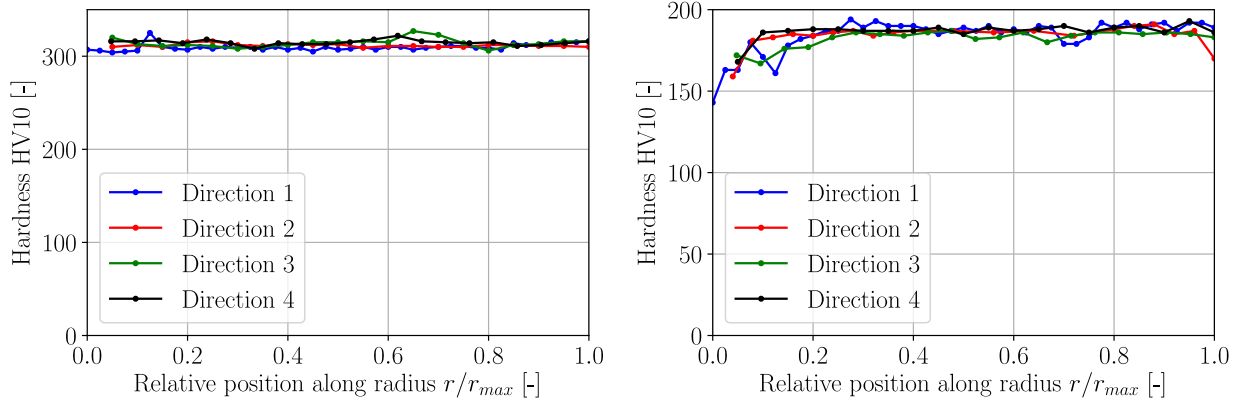


Figure 3: Hardness measurement Ti6Al4V(left) and Ck45 (right).

#### 2.4. Microstructure

The microstructure of the two materials is investigated by optical analysis of the etched surface and EBSD-analysis. This investigation should indicate possible irregularities of the grain structure or anisotropy in the material which could lead to different requirements for the constitutive model to be used in numerical simulations of the cutting experiments.

##### 2.4.1. Etching

Etched samples are prepared for microstructural analyses of the top and side surface. The Ti6Al4V samples are etched with Kroll. The microstructure of the top and side surface are shown in Figure 4. Due to the heat treatment both show a uniform microstructure without any salience.

The Ck45 is etched with Nital. Figure 5 shows the top surface. A ferritic-perlitic microstructure is visible. Towards the outer surface, decarburations and mill scales can be seen. At the disk center the microstructure is uniform. The side surface microstructure revealed a columnar structure along the cylinder axis, see Figure 6. This is likely to have been induced by rolling during the manufacturing process.

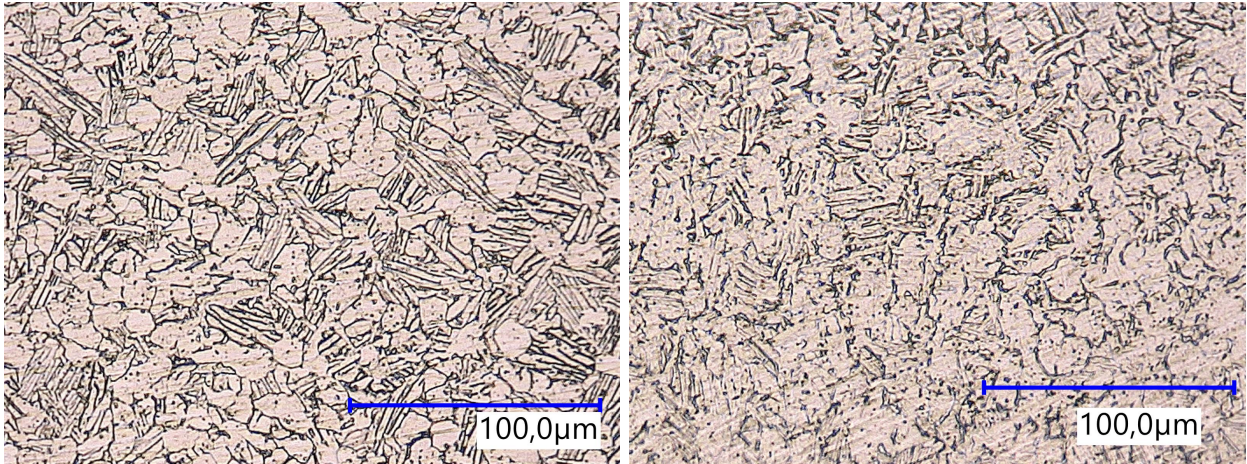


Figure 4: Microstructure of Ti6Al4V: the top surface (left) and the side surface (right) show a uniform grain structure.

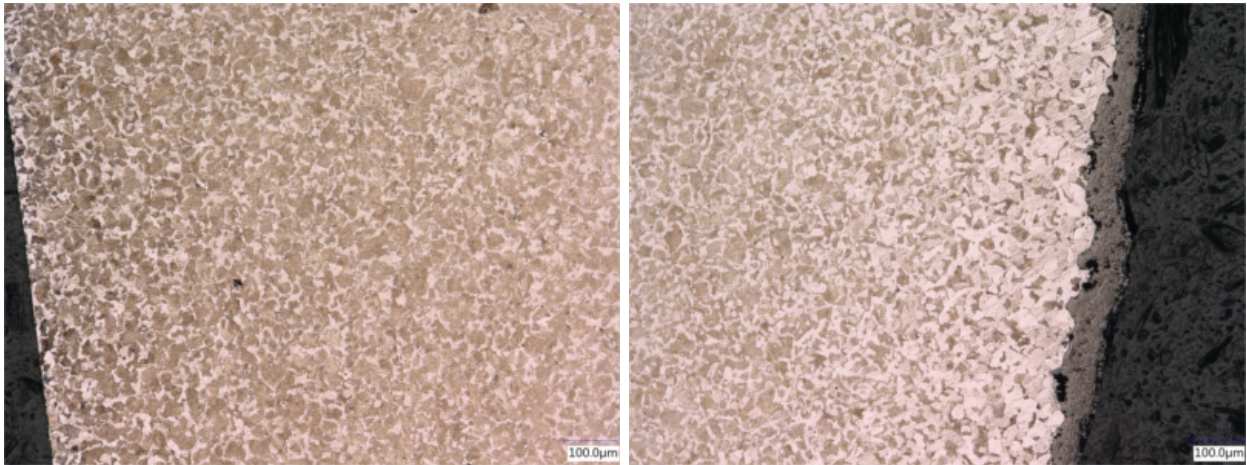


Figure 5: Microstructure of Ck45 steel: top surface at the disk center (left) showing a uniform grain structure and at outer radius (right) showing decarburization and mill scale.



Figure 6: Microstructure of Ck45 steel: side surface showing a columnar structure.

### 2.4.2. EBSD

The crystallographic orientations in the grains and the textures are measured with EBSD for the top and side surfaces of the Ck45 and Ti6Al4V material. The measured areas of the samples are given in table 4. The EBSD-analysis of Ti6Al4V reveals a slightly different ratio of  $\alpha$ - and  $\beta$ -phase for top and side surface. The average grain diameter and average aspect ratios of the grains are similar for the side and top surface. The results, together with grain sizes and aspect ratios, are given in table 5 for Ti6Al4V and Ck45. The grain orientations of Ti6Al4V are shown for the side and top surface in Figure 7, the corresponding distributions of  $\alpha$  and  $\beta$ -phases in Figure 8. The pole figures of the  $\alpha$ -phases are given with Figures 9 for side and top surface, respectively. The pole figures reveal a slightly stronger texture in the side surface than in the top surface. The grain orientations of Ck45 are shown for the top and side surface in Figure 10 and the pole figures in Figure 11. Similar to Ti6Al4V, the side surface shows a stronger texture than the top surface which may have been induced by the rolling process during manufacturing.

Specimen	Surface	Sample size [ $\mu m^2$ ]	Figures
Ti6Al4V	Side surface	443 x 347	7, 8, 9
Ti6Al4V	Top surface	331 x 428	
Ck45	Side surface	545 x 428	10, 11
Ck45	Top surface	709 x 556	

Table 4: EBSD measurement sizes of the four specimen.

Material	Surface	Avg. equiv. grain diameter $D_g$ [ $\mu m$ ]	Std.dev. $\mu_{D_g}$ [ $\mu m$ ]	Avg. grain aspect ratio	Std. dev. grain aspect ratio	$\alpha$ -phase vol. %	$\beta$ -phase vol.%	Comment
Ti6Al4V	Side surface	9.9	4.2	1.8	0.6	96.7	3.3	noisy raw data
Ti6Al4V	Top surface	9.1	3.2	1.7	0.5	94.8	5.2	
Ck45	Side surface	17.8	13.5	1.8	0.5	-	-	
Ck45	Top surface	14.3	9.3	1.8	0.6	-	-	

Table 5: Ti6Al4V and Ck45: EBSD measurement results for side and top surface.

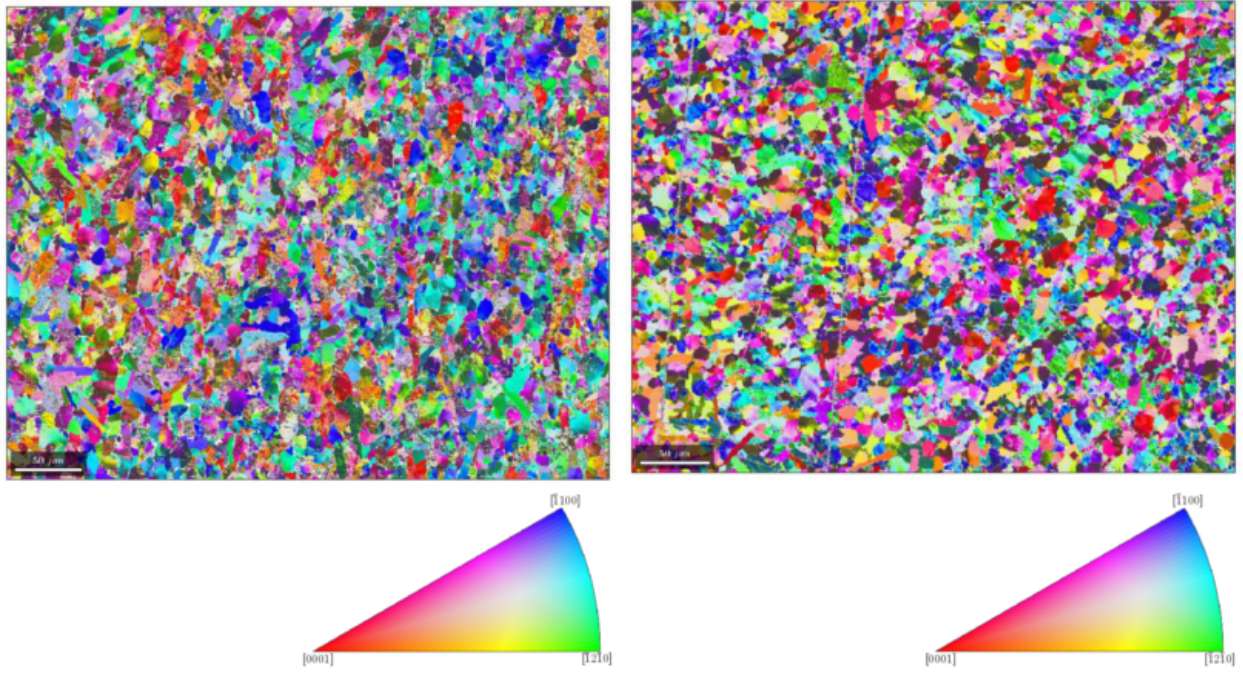


Figure 7: EBSD of Ti6Al4V: side (left) and top (right) surface with crystal orientations.

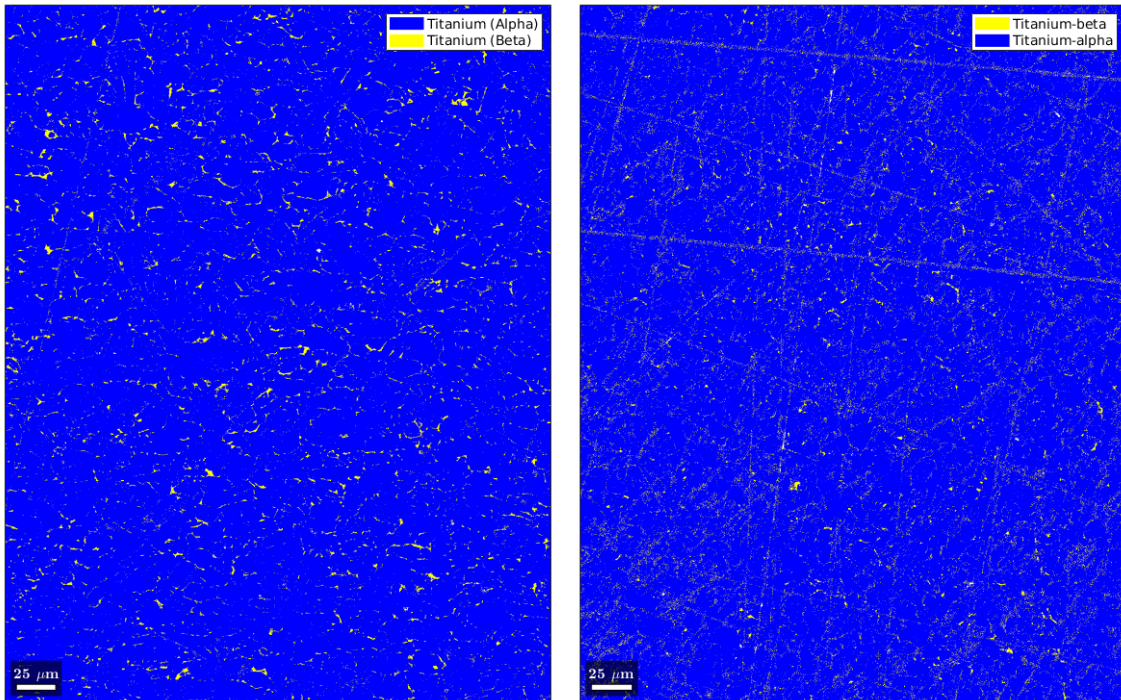


Figure 8: EBSD of Ti6Al4V:  $\alpha$  /  $\beta$ - phase distribution in the side (left) and top (right) surface.

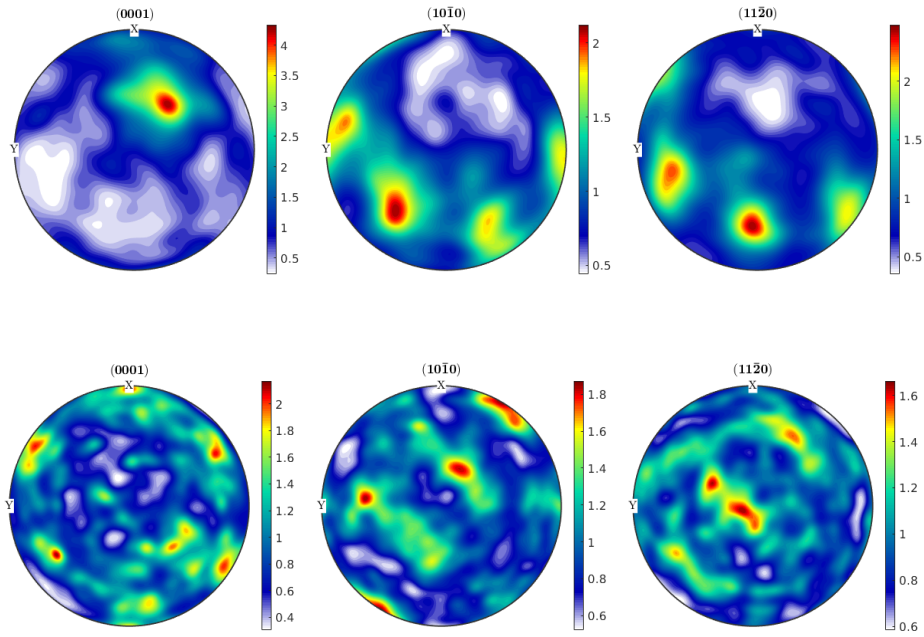


Figure 9: EBSD of Ti6Al4V: side (top row) and top (bottom row) surface pole figures of the  $\alpha$ - phase.

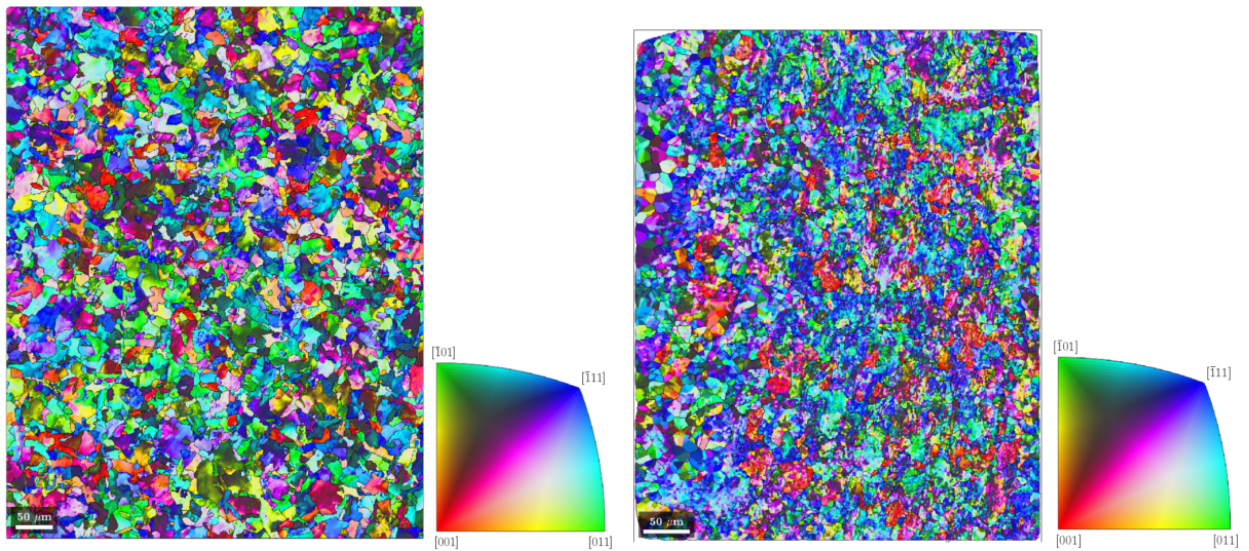


Figure 10: EBSD of Ck45: top (left) and side (right) surface with crystal orientations.

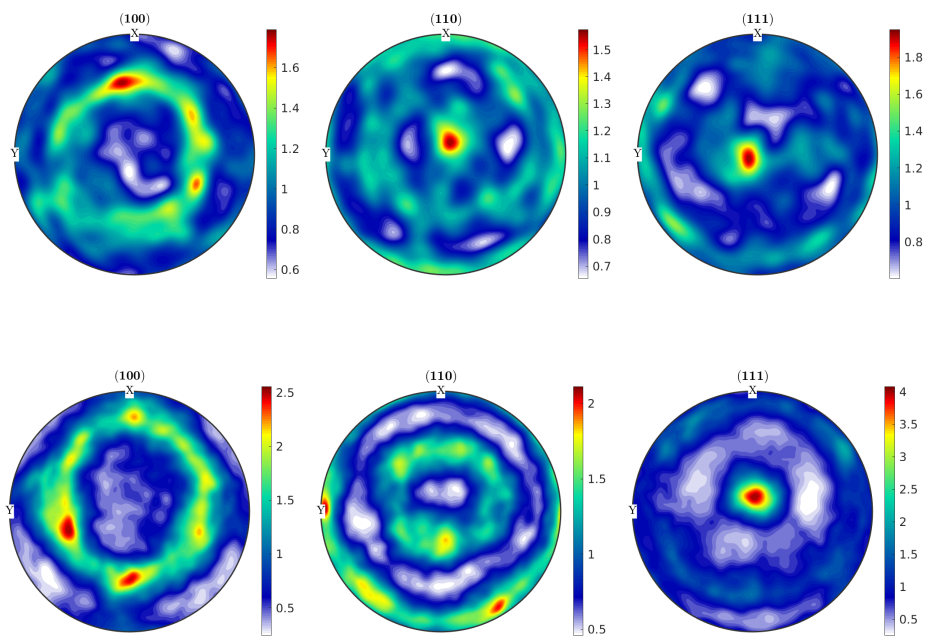


Figure 11: EBSD of Ck45: top (top row) and side (bottom row) surface pole figure.

## 2.5. Tensile Tests

In the following, tensile test results on this batch of materials are summarized from [19]. The tensile tests are performed for both materials, Ck45 and Ti6Al4V, at room temperature for three different strain rates ( $\dot{\varepsilon}_{pl} = 0.002 \text{ s}^{-1}, 0.1 \text{ s}^{-1}, 0.15 \text{ s}^{-1}$ ) and each repeated three times. The tensile test specimens are produced from the inner core of the cylinders according to DIN50125 [8] with form B and the dimensions B8x40. The tensile tests are used to fit material parameters for the work hardening and strain rate sensitivity part of the Johnson-Cook flow stress model [16]:

$$\sigma_y = \underbrace{(A + B \cdot (\varepsilon_{pl})^n)}_{\text{work hardening}} \underbrace{\left(1 + C \cdot \ln \left(\frac{\dot{\varepsilon}_{pl}}{\dot{\varepsilon}_{pl}^0}\right)\right)}_{\text{strain rate sensitivity}} \underbrace{\left(1 - \left(\frac{T - T_{ref}}{T_f - T_{ref}}\right)^m\right)}_{\text{thermal softening}} \quad (1)$$

where  $A$ ,  $B$ ,  $C$ ,  $m$  and  $n$  are material dependent parameters,  $\varepsilon_{pl}$  is the equivalent plastic strain,  $\dot{\varepsilon}_{pl}$  the plastic strain rate,  $T$  the temperature,  $T_f$  the melting temperature and  $T_{ref}$  the reference temperature of the material tests. Tests at temperatures higher than room temperature are not carried out, therefore the parameter  $m$  leaves undetermined. The parameters  $A$ ,  $B$ ,  $C$  and  $n$  are determined with the procedure in [20]. The strain rate sensitivity parameter  $C$  is valid only at very low strain rates, as the tests are conducted in the strain rate range from  $0.002 \text{ s}^{-1}$  to  $0.15 \text{ s}^{-1}$ . The obtained Johnson-Cook parameters are given in table 6 and the approximated flow curves are given in Figure 12 for Ti6Al4V and Ck45. The curve fits of the strain rate sensitivities are shown in Figure 13.

Material	A [MPa]	B [MPa]	n [-]	$\dot{\varepsilon}_{pl}^{ref}$ [s]	C [-]
Ti6Al4V	867	344	0.361	0.002	0.0145
Ck45	392	735	0.304	0.002	0.0108

Table 6: Ti6Al4V and Ck45: fit of the work hardening parameters  $A$ ,  $B$  and  $n$  and the strain rate sensitivity  $C$  of the JC flow stress model (1).

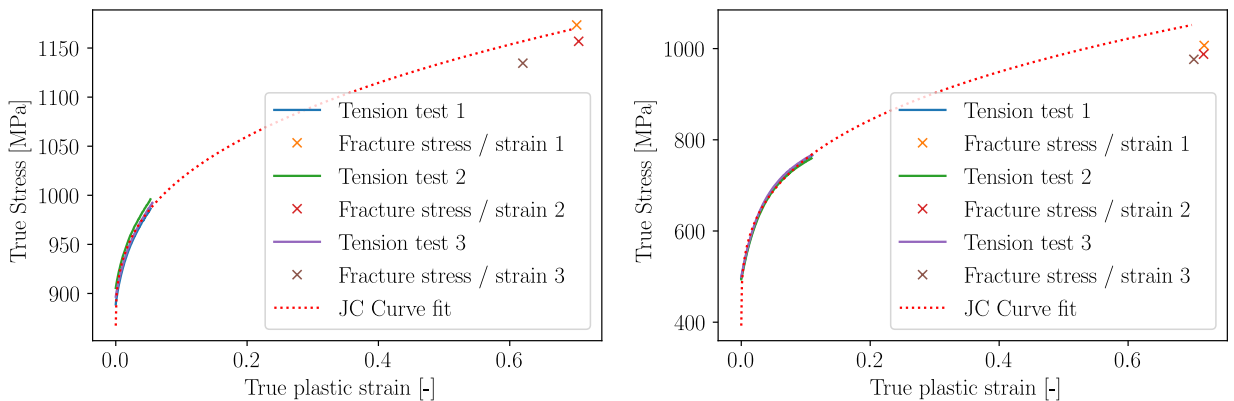


Figure 12: Fit of the Johnson-Cook parameters  $A$ ,  $B$  and  $n$  for quasi-static conditions ( $\dot{\varepsilon}_{pl} = 0.002 \text{ s}^{-1}$ ) for Ti6Al4V (left) and Ck45 (right).

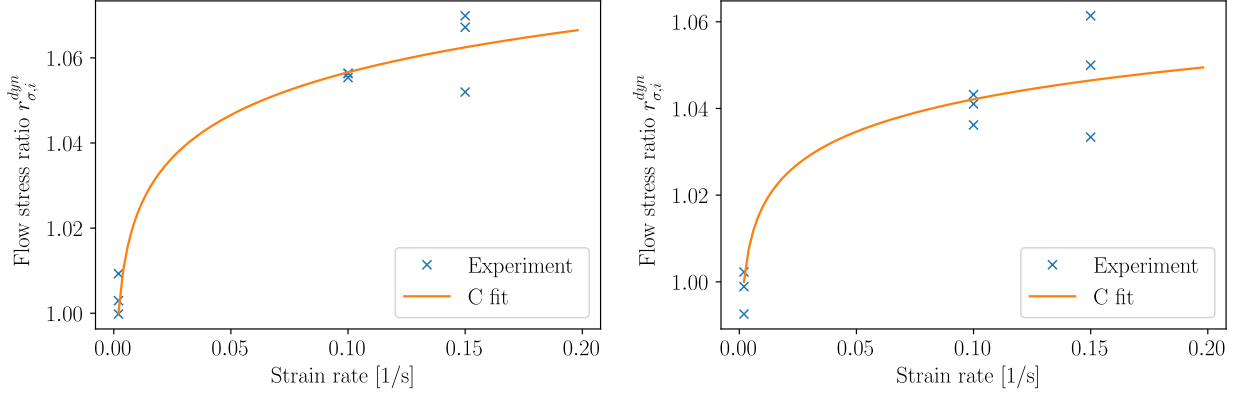


Figure 13: Fit of the Johnson-Cook strain rate sensitivity parameter C for Ti6Al4V (left) and Ck45 (right).

## 2.6. Cutting Tests

For the machining test, thin-walled cylinders with a diameter of  $D \approx 72$  mm and a wall thickness of  $d \approx 2$  mm are turned longitudinally on a Schaublin 42L CNC lathe. This emulates an orthogonal cut closely. The cylinders are turned inside and outside from the raw workpieces in the same clamping setup. The machining of the outer surfaces removes the scaling and the decarburated zone of the Ck45. The setup with a cylinder in place is shown in Figure 15 together with the experimental setup for the orthogonal cutting tests. Forces are measured using a Kistler 9121A5 dynamometer in combination with a Kistler 5019A charge amplifier and digitalized with a NI USB-6211 data acquisition system. The signal is low-pass filtered with a cut-off frequency of 30 Hz before being sampled with 1.1 kHz. Offset and drift in the measured force signal  $\tilde{F}_{meas}$  are corrected after the measurement since small drifts  $\tilde{F}_{drift}$  in the signal can occur and overlay the process forces  $\tilde{F}_{proc}$ :

$$\tilde{F}_{proc} = \tilde{F}_{meas} - \tilde{F}_{drift} \quad (2)$$

The drift  $\tilde{F}_{drift}$  of the force is evaluated by positioning the cutter before the cut with a distance of one mm away from the cylinder to cut. With the desired feed rate of the experiment the cutter approached the workpiece and during this time the idle-forces  $\tilde{F}_{drift} = \tilde{F}_{idle}$  are recorded and then used to correct to force signals with (2). A schematics of this correction is shown in Figure 14.

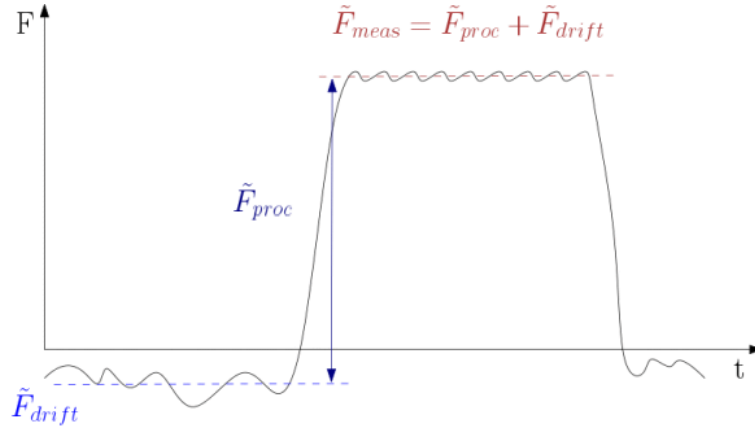


Figure 14: Force signal overlaid with a drift.

High speed camera recordings are conducted for the first cutting tests with a Phantom V12.1 camera using an endoscope, see the cutting setup in Figure 15. References to these records are linked in the result tables B.14 and B.15. In order to simplify numerical modelling, the experiments are performed as dry cuts without the use of a lubricant. To date no viable approach for considering coolant and lubricant in numerical modeling exists, and the use of dry sections reduces the number of unknown parameters. Each combination of feed  $f$  and cutting speed  $v_c$  is usually tested three times to ensure results quality and repeatability. For each test an unused cutting edge is used and test durations are kept short so that wear stays insignificant.

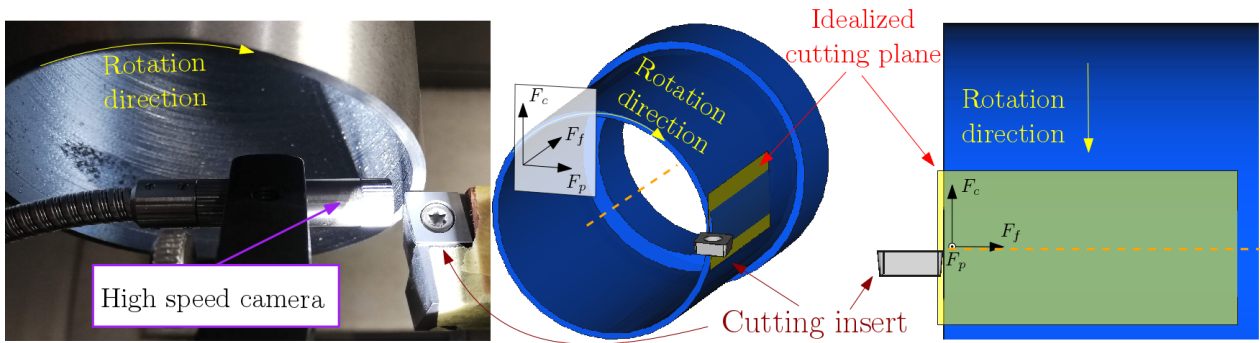


Figure 15: Quasi-orthogonal cutting setup: cylinder with cutting insert (left and middle), cutting plane in 2D (right).

Uncoated turning inserts *Sandvik Coromant* CCMW 09T304 H13A (ISO) are used for the cutting experiments. The main geometrical data of the inserts are given in table 7 and pictures of the turning insert geometry are provided in Figure 16.

Edge radius RE	Cutting edge height S	Inscribed circle IC	Cutting edge length LE	Clearance angle $\alpha$	Rake angle $\gamma$	Cutting edge radius
0.397mm	3.969mm	9.525mm	9.272mm	7°	0°	see chapter 2.6.1

Table 7: Main geometry data of *Sandvik Coromant* CCMW 09T304 H13A (ISO) inserts.

The cutting edge radii along the cutting edge length LE result from the sintering process and exhibit a certain scatter. Since these radii have a significant impact on the process forces, they are optically measured, see details in chapter 2.6.1. An Applitec SCACL-2020X-09 tool

holder (ISO-2216) is used, which has an entering angle  $\xi = 90^\circ$  and an inclination angle  $\kappa = 0^\circ$ . Each insert is used for four cutting experiments (two cuts per side of the insert) where after every experiment another position A-D was used on the insert. These four cut positions A-D are shown in Figure 16.

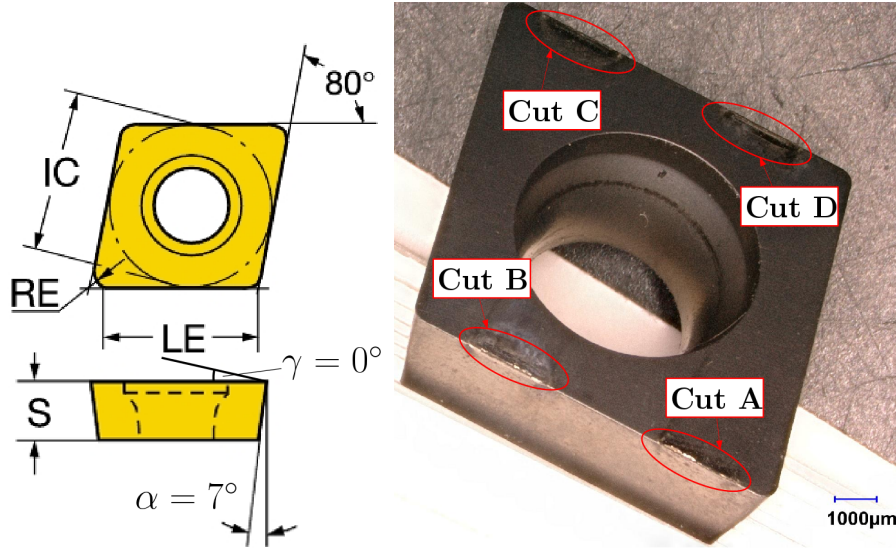


Figure 16: Cutting insert geometry (left) from [32] and four cut positions A-D (right) for cutting experiments, from [19].

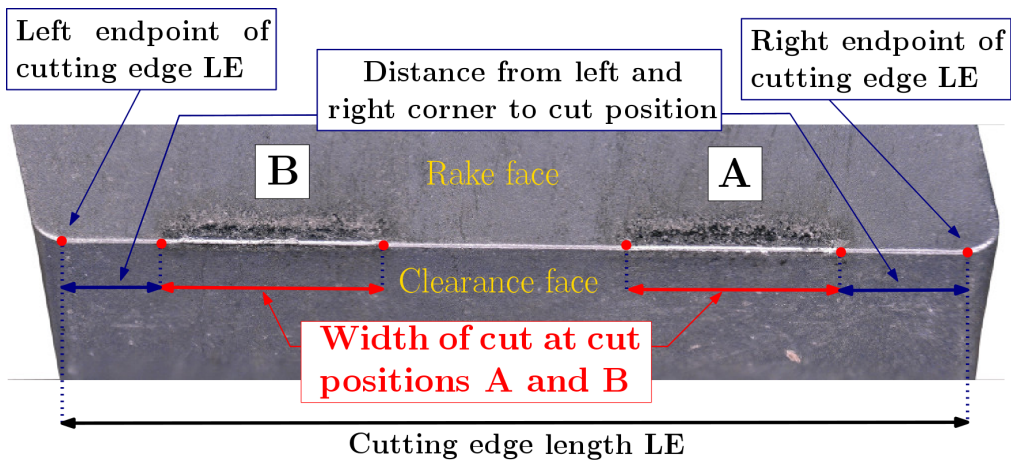


Figure 17: Cutting insert with cut positions A and B showing start and endpoints of the cutting edge, shortest distances from the corners to the beginning of the cutting zones and width of cuts.

### 2.6.1. Determination of Cutting Edge Radii

The shape of the cutting insert, especially the cutting edge radius, have a major influence on the process forces of the turning operation. Albrecht [1] showed for steel that with increasing cutting edge radius the feed force  $F_f$  increases strongly and the cutting force  $F_c$  increases moderately. The effect becomes more pronounced with higher feeds. Wyen [38] conducted a similar investigation for Ti6Al4V revealing comparable influences on the process forces, see Figure 18.

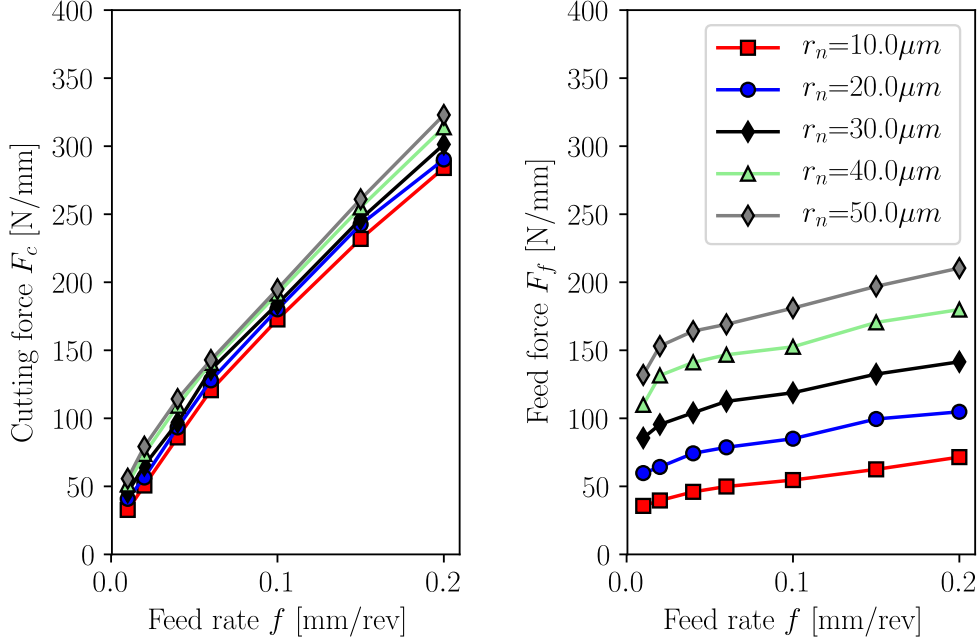


Figure 18: Influence of cutting edge radius  $r_n$  and feed  $f$  on the cutting and feed forces for turning of Ti6Al4V. The forces are standardised to a cut width of  $b = 1$  mm, the cut speed was  $v_c = 70$  m/min, the rake angle  $\gamma = 10^\circ$  and the clearance angle  $\alpha = 8^\circ$  according to measurements from [38].

The inserts in this investigation have an unspecified cutting edge radius and therefore all cutting edges (2 x 149 inserts) of the cutting inserts are optically measured with an Alicona InfiniteFocusG4 microscope prior to the cut tests in an unused condition. With the focus variation principle [6, 21], 3D data of the scanned surfaces are generated, where a 20x magnification with  $0.5 \mu\text{m}$  vertical and  $7 \mu\text{m}$  lateral resolution is used to scan along the complete cutting edge length (LE). Initially a scan depth of  $60 \mu\text{m}$  was used but since in some positions cutting edge radii of about  $50 \mu\text{m}$  appeared, it was then later increased to  $400 \mu\text{m}$ . Before the cutting edge radii determination the scanned 3D data is reworked. In a first step single peaks (measurement artefacts) are removed. This is followed by the determination of the left and right endpoints of the cutting edge (LE) between the corner radii for which height profile gradients are evaluated. In between these two points the cutting edge radii are analyzed and they serve as reference points for the exact determination of the cut position after the experiments.

The determination of the cutting edge radii follows the procedures outlined in [23, 40] in order to ensure reproducibility of the results. A total of about 1'275'000 cutting edge radii ( $> 4000$  radii per cutting edge) are extracted from the scans. Over all 149 cutting inserts, the cutting edge radius along LE varies between  $\approx 20 \mu\text{m}$  and  $\approx 50 \mu\text{m}$ . The variation of the cutting edge radius along one cutting edge length  $LE$  can be significant, as for instance shown in Figure 20, where it varies between  $r_n \approx 25 \mu\text{m}$  and  $r_n \approx 50 \mu\text{m}$ . The mean cutting edge radius is  $37.5 \mu\text{m}$  with a standard deviation  $4.9 \mu\text{m}$ . The scatter of the radius is the reason, why the exact cutting edge radius was determined after the experiments, when the location of the cut on the cutting edge is known for every insert and its four cut positions A-D. The insert's edge radii serve as reference points to determine the start point of the cut positions. From this start point the cutting edge radii are averaged along the cut width of  $\approx 2$  mm. Its averaged values along the cut width, including the standard deviation, are given for each cutting experiment in tables B.14 and B.15. Histogram plots of the cutting edge

length  $LE$  and the cutting edge radii are given in Figure 19. The length of the cutting edge  $LE$  varies between  $\approx 8.7$  mm and  $\approx 8.95$  mm which is inline with the tolerance class of the selected inserts.

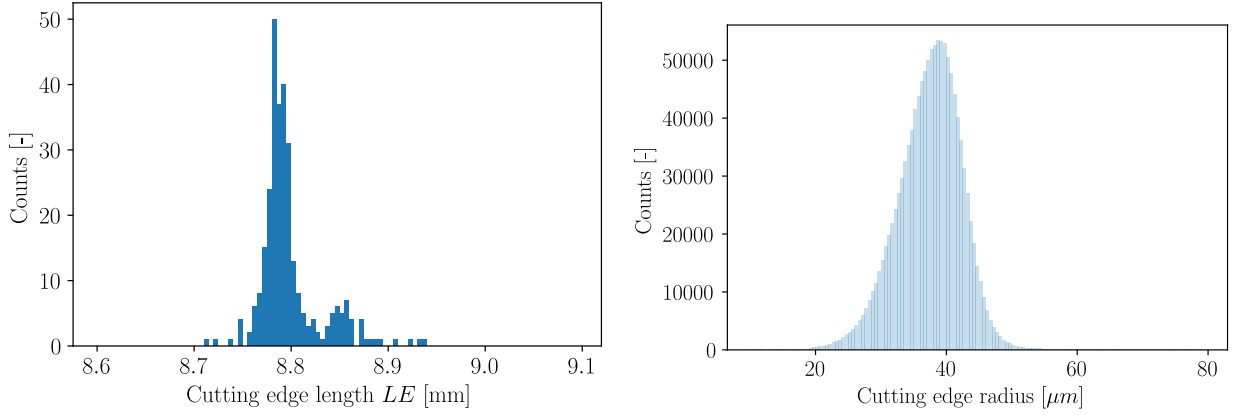


Figure 19: Histogram of cutting edge lengths  $LE$  (left) and cutting edge radii (right) over all cutting inserts.

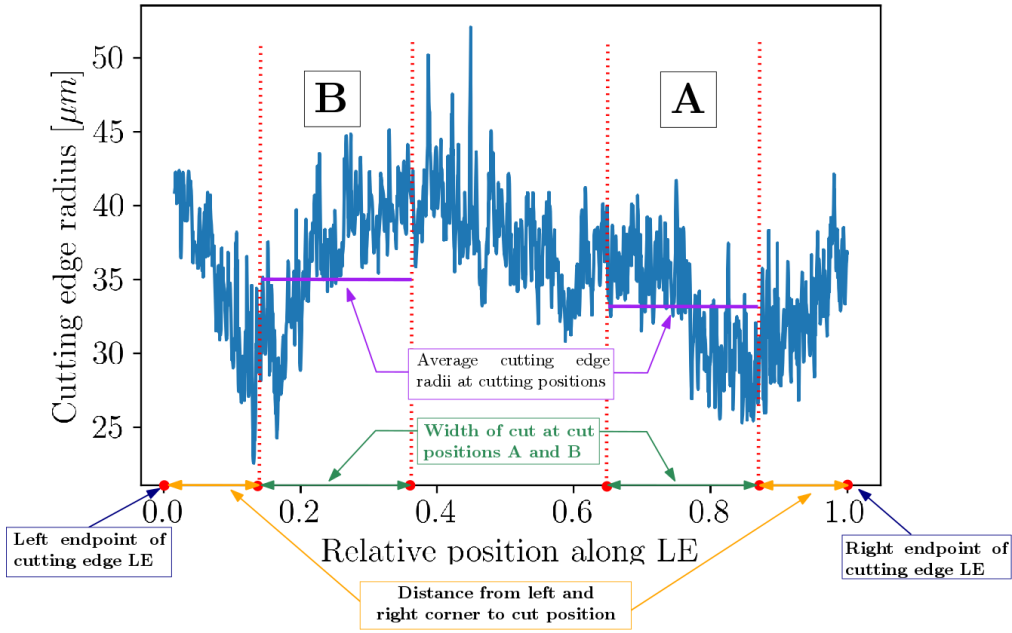


Figure 20: Example of cutting edge radii variation along a single cutting edge, with averaged cutting edge radii at cut positions A and B.

### 2.6.2. Chip Thickness Measurements

At least one chip from the three repetitions of each set of feed  $f$  and cut speed  $v_c$  is embedded, ground (120, 240, 500, 1000, 2500, 4000) and polished ( $6\mu\text{m}$ ,  $3\mu\text{m}$ ,  $1\mu\text{m}$ ). After polishing, the chips are etched with Kroll (Ti6Al4V) and Nital (Ck45). The geometry and microstructure are then analysed with a Keyence VHX-5000 microscope. The main dimensions which are measured are the chip area  $A_{chip}$  and the unrolled chip length  $l_{chip}$ , see Figure 21, from which the average chip thickness  $h_{avg}$  is computed as:

$$h_{avg} = \frac{A_{chip}}{l_{chip}} \quad (3)$$

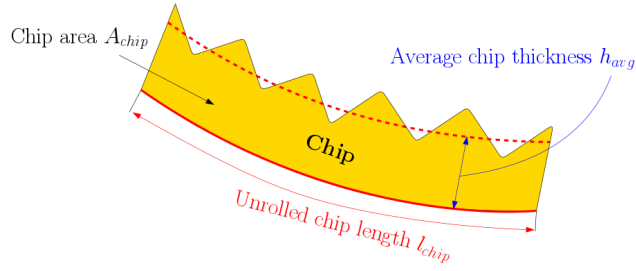


Figure 21: Measurement of average chip thicknesses  $h_{avg}$  by the chip area  $A_{chip}$  and unrolled chip length  $l_{chip}$ .

### 2.6.3. Test Plan

Orthogonal cutting tests are conducted for a large range of feed and cutting speeds. Each experimental set is repeated three times to ensure the reproducibility of the results. In total 520 cutting tests are conducted, of which 288 are for Ti6Al4V and 232 for Ck45, respectively. The parameter ranges are given in table 8 and all combinations of feed  $f$  and cutting speeds  $v_c$  which are used in the cutting experiments of Ti6Al4V and Ck45 are displayed in Figure 22.

Material	Cutting speed $v_c$ [m/min]	Feed rate $f$ [mm/rev]
Ti6Al4V	10...500	0.01...0.4
Ck45	10...500	0.01...0.4

Table 8: Test matrix of the cutting tests

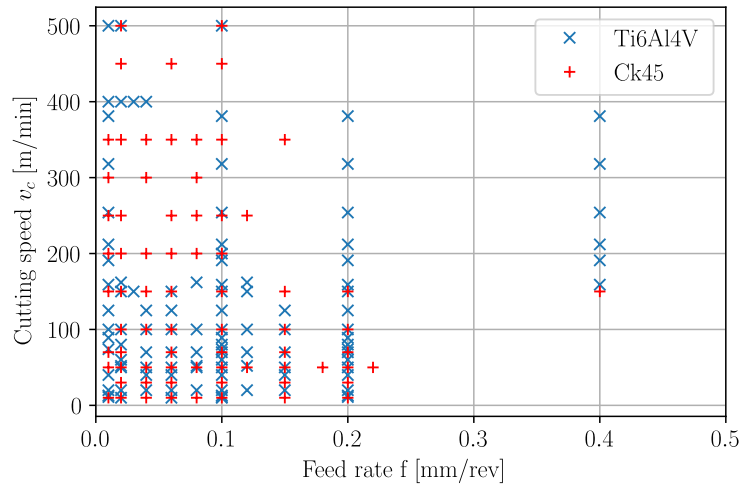


Figure 22: Process parameter combinations used in the orthogonal cutting experiments.

## 3. Results

Tables A.12 and A.13 in the appendix list the process parameters for each experiment ID and indicates for which experiments chip thicknesses are measured and for which etched

samples are documented. The complete cutting test results are provided for Ti6Al4V in table B.14 and for Ck45 in table B.15 in the Appendix B. The process forces  $F_c$  and  $F_f$  are normalized to a cutting width of  $w = 1\text{mm}$  and are given together with their respective standard deviations  $\sigma_{F_c}$  and  $\sigma_{F_f}$ . The next two columns contain the averaged cutting edge radius  $r_n$  and its standard deviation  $\sigma_{r_n}$ , followed by the average chip thickness  $h_{avg}$  and its standard deviation  $\sigma_{h_{avg}}$  (if more than one chip is evaluated), the cutting distance  $l_{cut}$  and the temperature of the chip  $T_{chip}$  derived from the tempering color (only Ck45). The last two columns contain a qualitative statement of the tool wear and the quality of the process forces measurement.

### 3.1. Process Forces

The experimentally measured process forces are displayed in in Figure 23 for Ti6Al4V and in Figure 24 for Ck45. The colour of the dots indicates the cutting edge radius  $r_n$  or cutting speed  $v_c$  of the respective experiment. For Ti6Al4V, cutting and feed force increase with increasing feed. The cutting forces  $F_c$  tend to increase with increasing cutting edge radius  $r_n$  but decrease towards higher cutting speed  $v_c$ . The feed force  $F_f$  increases as well with increasing  $r_n$ , but increasing  $v_c$  leads to higher forces only until feeds around  $f = 0.1\text{mm}$ .

The Ck45 exhibits a complex behaviour: the process forces increase as well with increasing feed but dependencies on the cutting edge radius  $r_n$  or cutting speed  $v_c$  are not obvious. Instead, at a constant feed the process forces first increase from very low to medium cutting speeds ( $v_c \approx 100\text{m/min}$ ) and then start to drop to similar low forces as with very low cutting speeds, see for example the feed forces at  $f = 0.1\text{mm}$  in Figure 24.

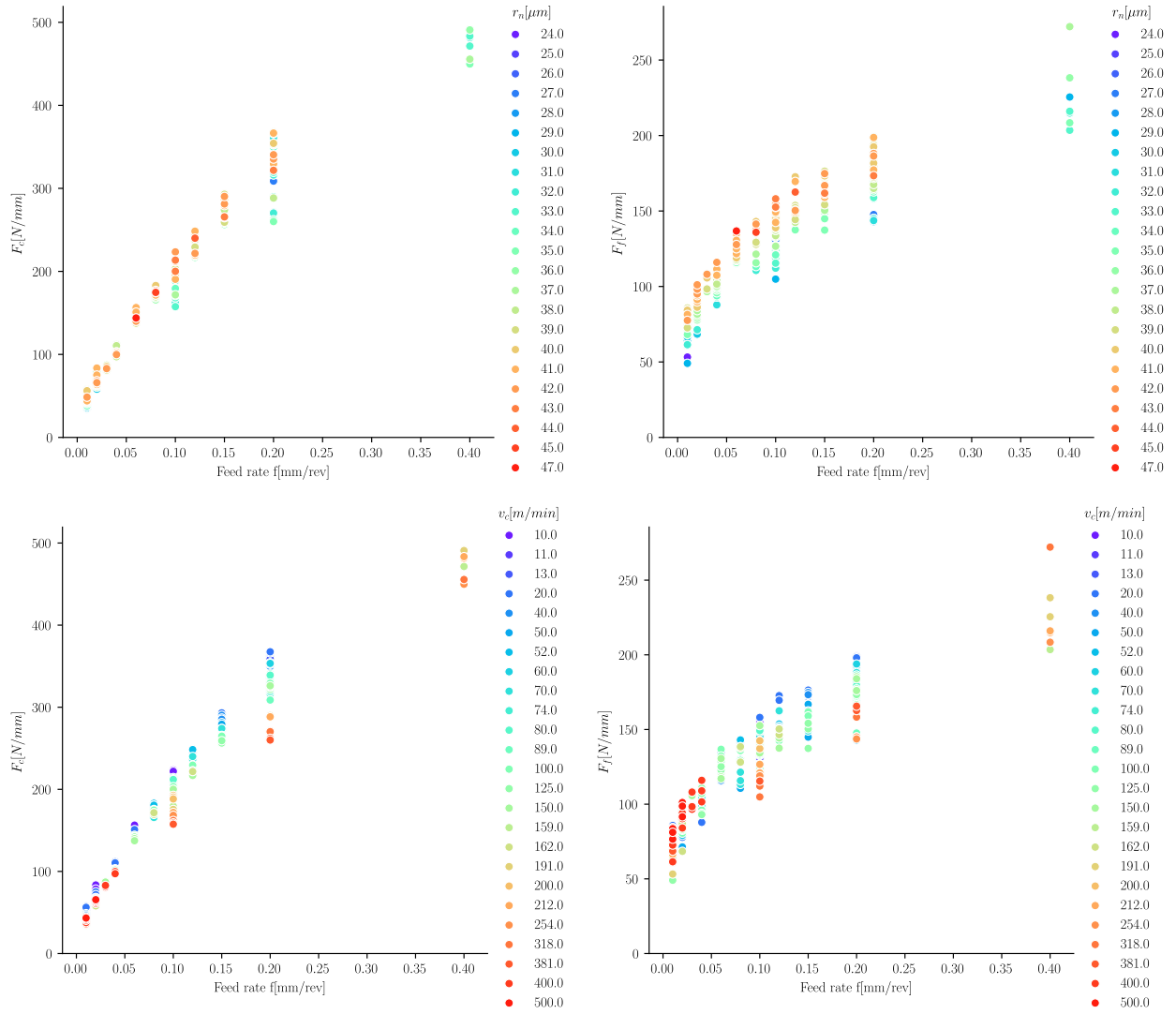


Figure 23: Process forces Ti6Al4V cutting experiments, cutting (left column) and feed force component (right column) depending on the feed  $f$ , the colour depicts the cutting edge radius  $r_n$  (top row) and the cutting speed  $v_c$  (bottom row) of the experiment.

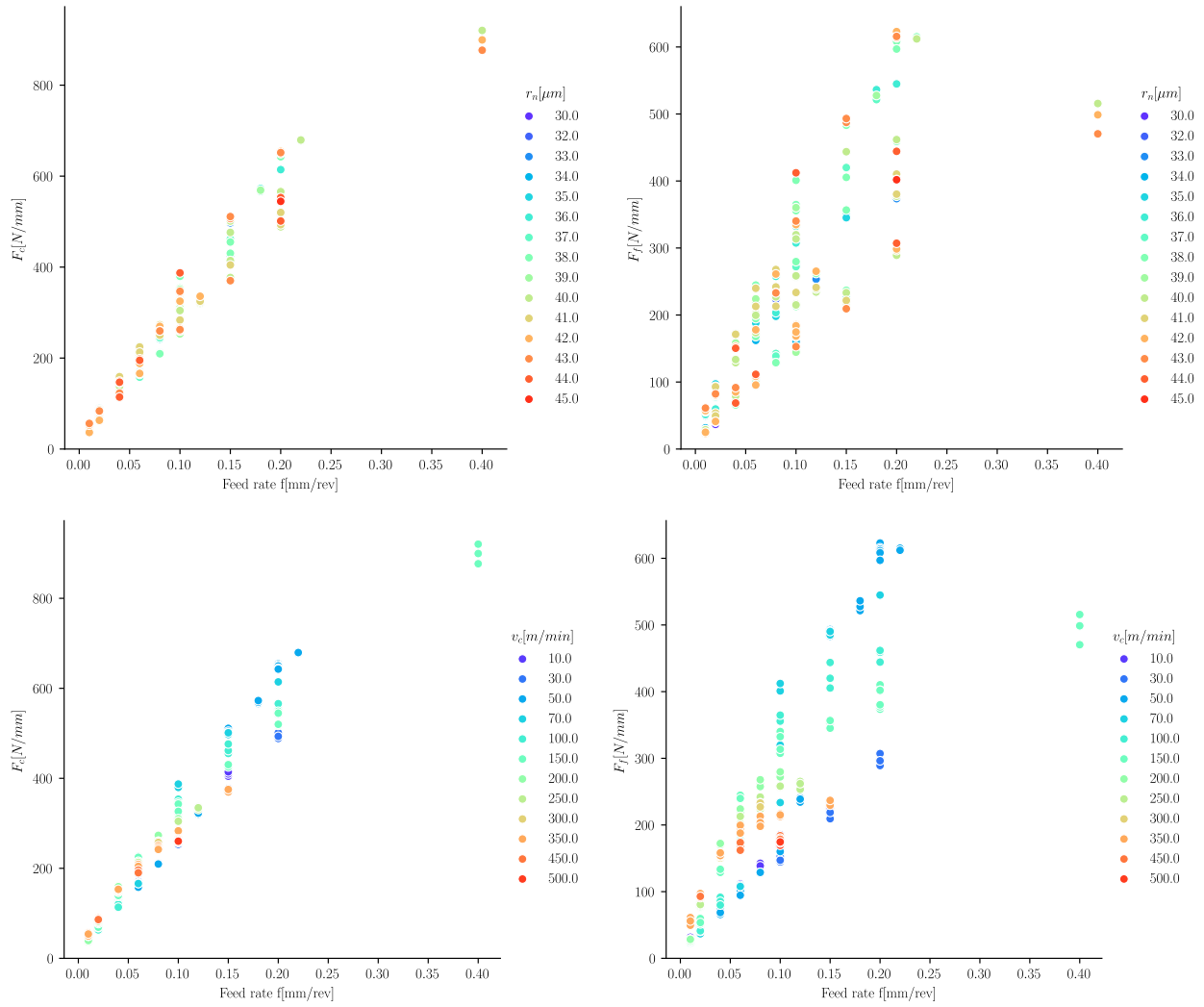


Figure 24: Process forces Ck45 cutting experiments, cutting (left column) and feed force component (right column) depending on the feed  $f$ , the colour depicts the cutting edge radius  $r_n$  (top row) and the cutting speed  $v_c$  (bottom row) of the experiment.

### 3.2. Chip Shapes

At least one chip sample of every feed rate and cutting speed combination is etched. In the following a small selection is shown for Ti6Al4V and Ck45. For Ti6Al4V, chips in a feed range of  $f = 0.01mm, 0.1mm$  and  $0.2mm$  and at cutting speeds of  $v_c = 11, 40, 191$  and  $381m/min$  are displayed in table 9. All chips show chip segmentation where towards higher feed  $f$  and higher cutting speed  $v_c$  the segmentation becomes more pronounced. In all Ti6Al4V cutting experiments chip segmentation occurred, but traces of the effect of built-up edges (BUE) cannot be identified on any of the chips.

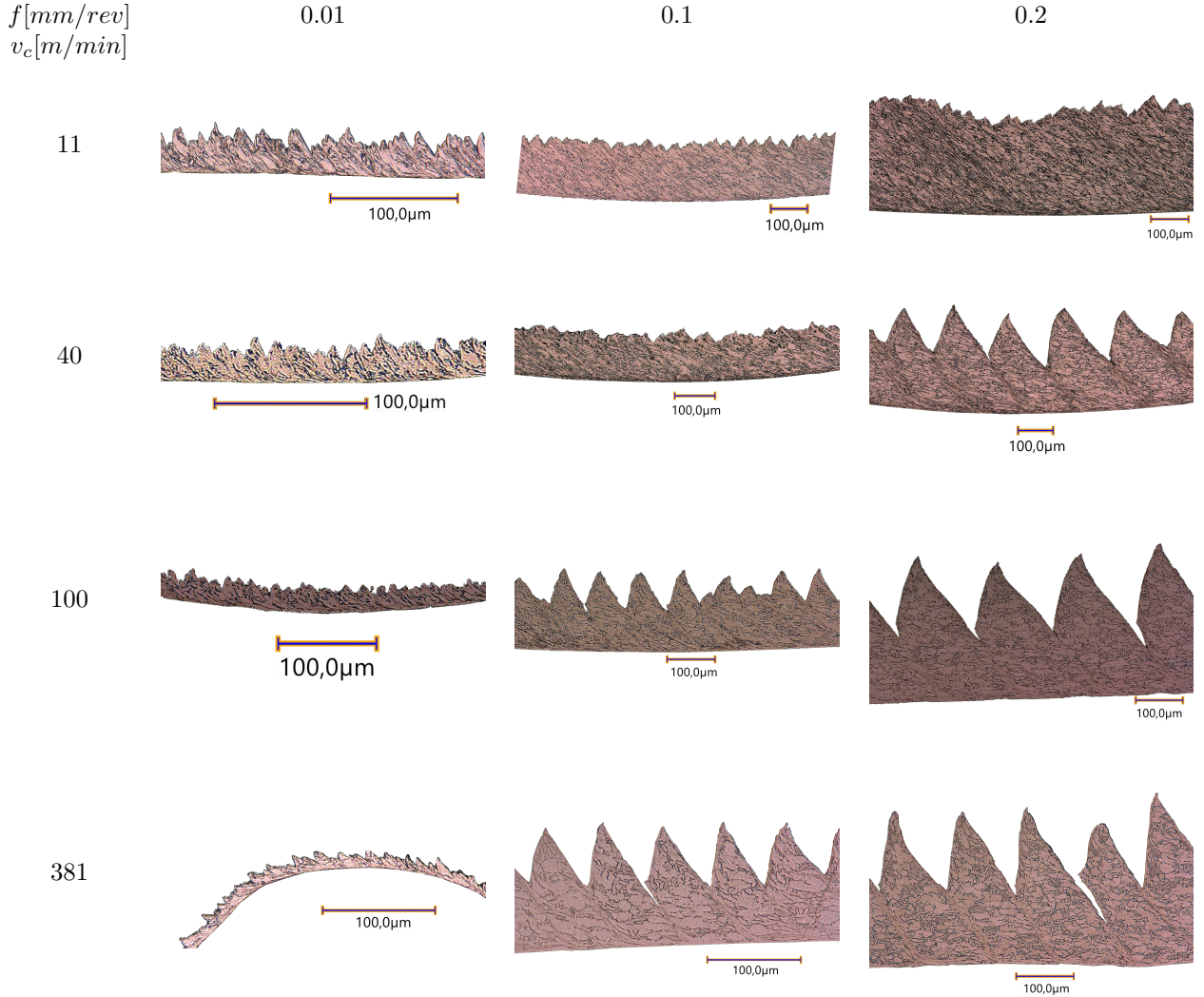


Table 9: Ti6Al4V: Chip overview of selected experiments with the chip flow direction in all images from right to left. Towards higher cuttings speed and higher feed rates the chip segmentation becomes more pronounced.

For Ck45, chips in a feed range of  $f = 0.02mm, 0.06mm$  and  $0.1mm$  and at cutting speeds of  $v_c = 10, 50, 150$  and  $450m/min$  are displayed in table 10. Ck45 chips show BUE traces in the chips up to  $v_c = 50m/min$  at all three feed levels, while at  $v_c = 150m/min$  only for  $f = 0.02mm$  BUE is visible and for  $v_c = 450m/min$  no BUE is visible at all. At higher cutting speeds and higher feeds of the Ck45 cutting experiments the BUE-formation diminishes, while chips segmentations start to form, see Figure 25.

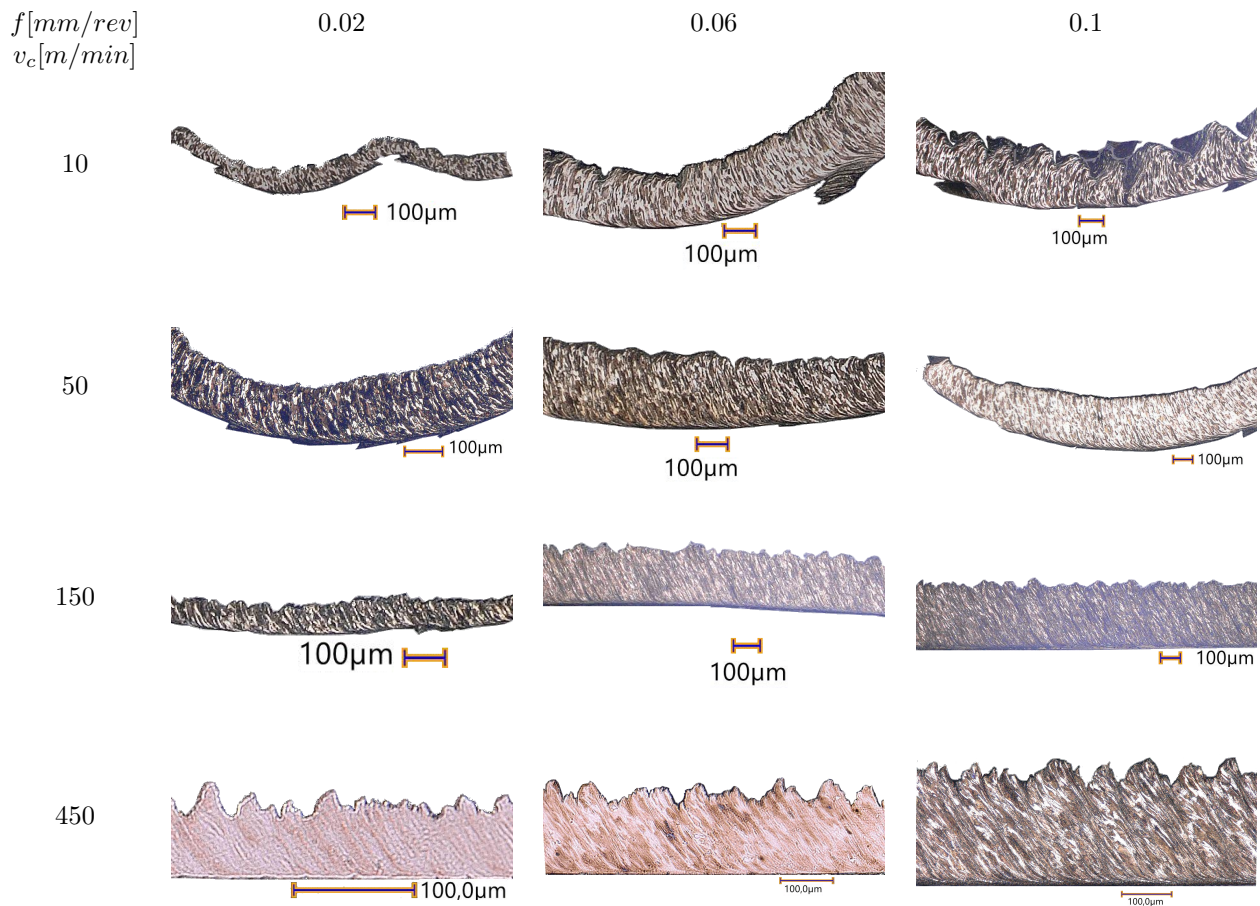


Table 10: Ck45: Chip overview of selected experiments with the chip flow direction in all images from right to left. Towards higher cuttings speed and higher feed rates chip segmentation starts to form, while traces of BUE diminish and disappear.

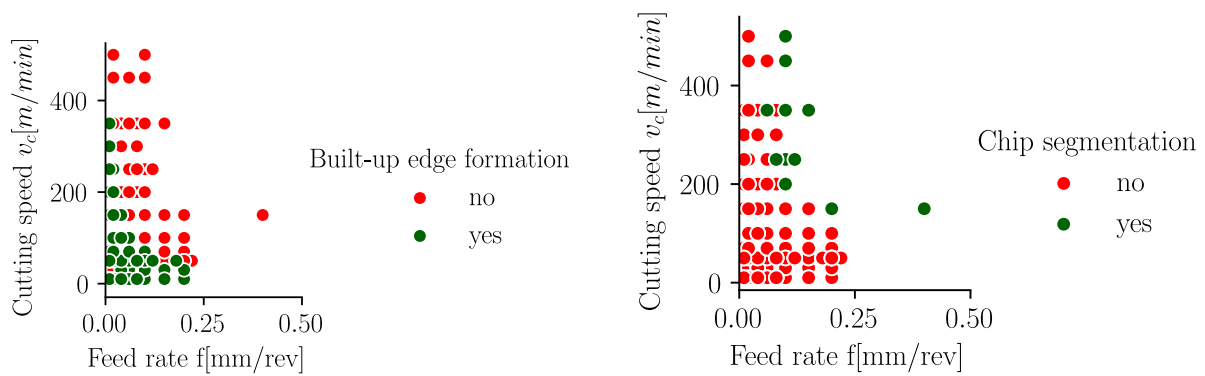


Figure 25: Built-up edge formation (left) and chip segmentation (right) in Ck45 depending on cutting speed  $v_c$  and feed  $f$ .

### 3.3. Chip Thicknesses

At least one chip of each combination of feed and cutting speed is embedded in Bakelite for the manual measurement of  $h_{avg}$  using the method described in chapter 2.6.2. The measured thicknesses are documented in the result tables B.14 (Ti6Al4V) and B.15 (Ck45). The average chip thicknesses show high scatter for Ti6Al4V and Ck45. For this reason trendlines are created for some selected feeds using the Savitzky-Golay filter [33] in SciPy [37]. A trend of decreasing chip thicknesses towards an increase of the cutting speed  $v_c$  at constant feed rate  $f$  is visible for both, Ti6Al4V and Ck45, see Figures 26 and 27, respectively. In case of Ck45, an initial increase of the average chip thickness with increasing cutting speed for feed rates  $f \geq 0.04$  mm is seen. However, upon further increase of the cutting speed, the average chip thickness decreases again. The cutting speed at which the behaviour reverses is not constant for all feed rates: as the feed increases, the maximum of the average chip thickness moves towards smaller cutting speeds  $v_c$ .

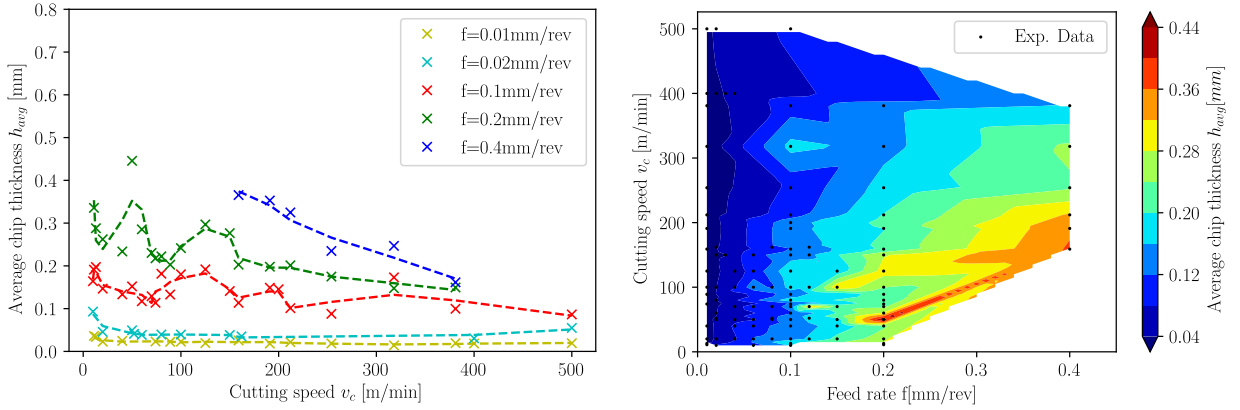


Figure 26: Measured average chip thicknesses of Ti6Al4V for different feeds  $f$  and varying cuttings speeds  $v_c$ . Evaluation for selected feed rates (left) and interpolated contour plot (right).

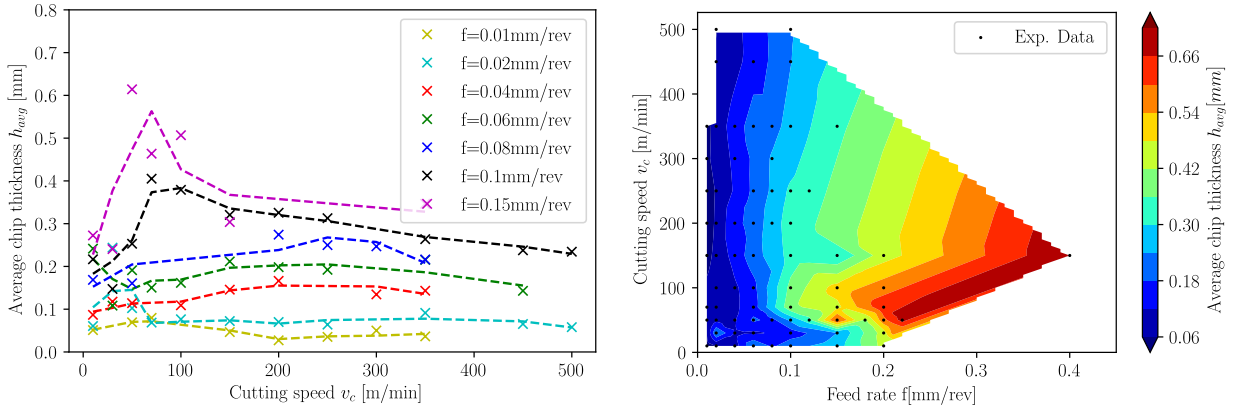


Figure 27: Measured average chip thicknesses of Ck45 for different feeds  $f$  and varying cuttings speeds  $v_c$ . Evaluation for selected feed rates (left) and interpolated contour plot (right).

The measured chip thicknesses show some scatter, the reasons could be due to:

- the manual measurement procedure,
- misalignments of chips in the embedding procedure because the chips are curled not only in feed direction but also due to the cylinder radius and

- low stiffness of thinner chips which could lead to skewing and therefore larger effective cross-sections after embedding.

The low stiffness of thinner chips prevented as well from the large scale evaluation of chip curling radii.

### 3.4. Friction Coefficient

The measured process forces in the cutting experiments can be used to deduce friction coefficients. The simplest estimation is based on the ratio of tangential and normal forces exerted on the tool, also known as apparent friction coefficient  $\mu_{app}$ . It is given according to Merchant [25, 26] as:

$$\mu_{app} = \frac{F_f + F_c \cdot \tan\gamma}{F_c - F_f \cdot \tan\gamma} \quad (4)$$

with  $F_f$  and  $F_c$  being the feed and cutting components of the process forces and  $\gamma$  being the rake angle. The drawback of the apparent friction coefficient  $\mu_{app}$  is the neglect of the cutting edge radius influence assuming an ideal sharp tool (perfect wedge). The apparent friction coefficients are shown for Ti6Al4V cutting experiments in Figure 28. Towards higher feeds the apparent friction coefficient decreases to levels of  $\mu_{app} \approx 0.4..0.6$ . Especially at very low feeds the cutting speed has a dominating influence on  $\mu_{app}$  while with increasing  $f$  the cutting edge radius  $r_n$  becomes more important.

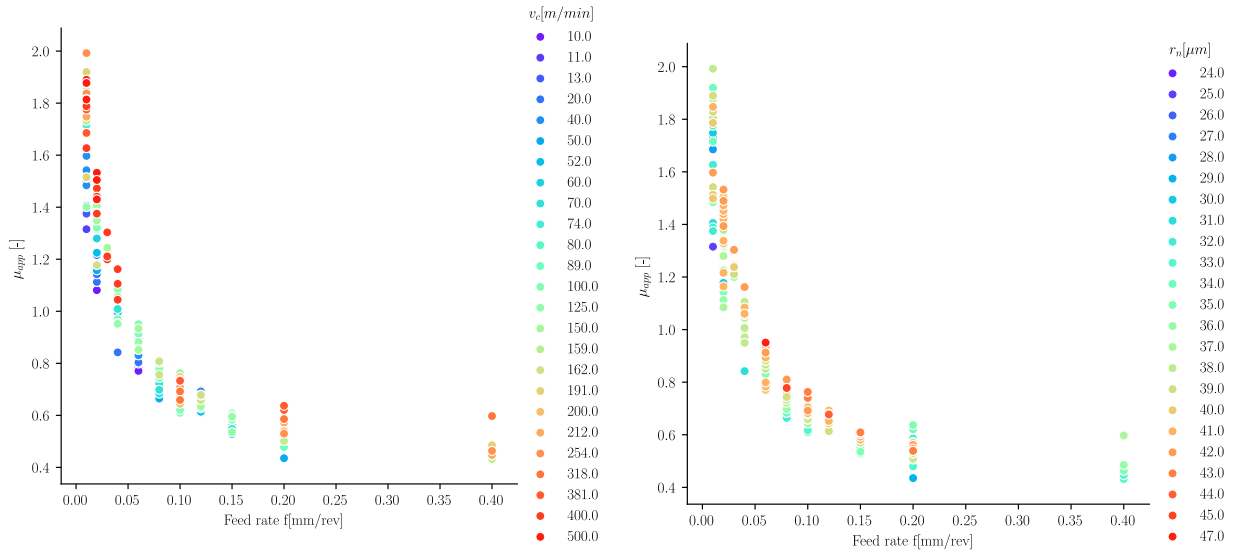


Figure 28: Apparent friction coefficients  $\mu_{app}$  versus feed  $f$  for Ti6Al4V . The colour indicates the cutting speed  $v_c$  (left) and the cutting edge radius  $r_n$  (right).  $\mu_{app}$  decreases with increasing feed  $f$  and decreasing cutting speed  $v_c$ .

The apparent friction coefficients of the Ck45 cutting experiments are shown in Figure 29. The cutting edge radius  $r_n$  plays no obvious role in  $\mu_{app}$ , but for very low  $f$  and increasing cutting speed  $v_c$  an increase in  $\mu_{app}$  is visible which then drops upon further increases in  $v_c$ . This behaviour is likely due to a change in BUE-formation and chip segmentation which changes towards increasing  $f$  and  $v_c$ , see also Figure 25.

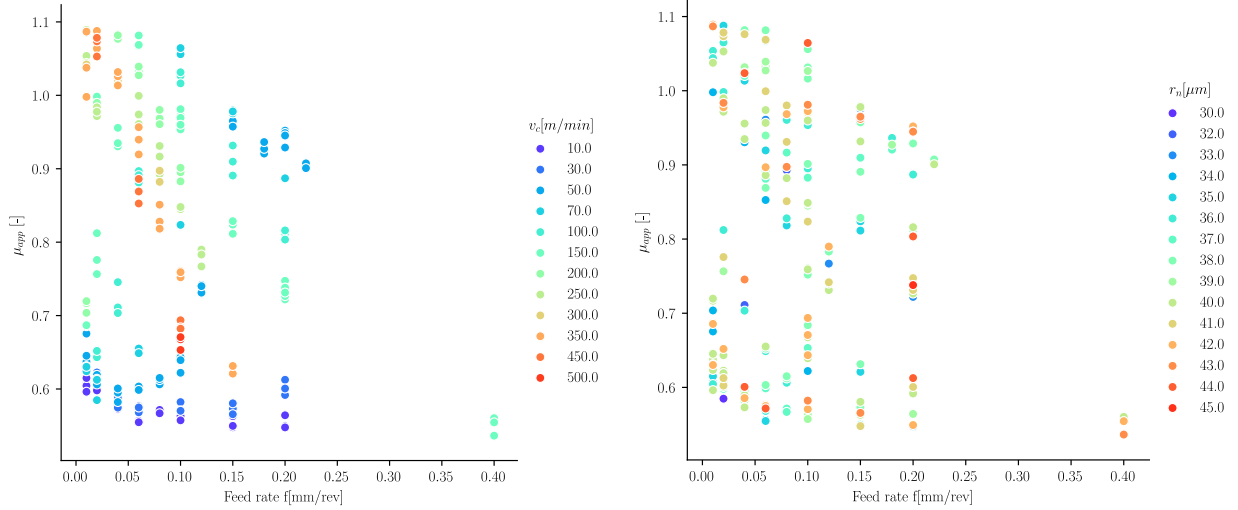


Figure 29: Apparent friction coefficients  $\mu_{app}$  versus feed  $f$  for Ck45. The colour indicates the cutting speed  $v_c$  (left) and the cutting edge radius  $r_n$  (right). A dependency on the cutting edge radius  $r_n$  is not visible, while for very low  $f$  and increasing cutting speed  $v_c$  an increase in  $\mu_{app}$  is visible which then drops upon further increases in  $v_c$ . This behaviour is likely due to a change in BUE-formation and chip segmentation.

A more elaborated approach for the determination of the friction coefficient from cutting experiments is described by Albrecht [1], considering the ploughing effect due to finite sharpness effect in the determination of the friction coefficient  $\mu_{fr}$ :

$$\mu_{fr} = \frac{(F_f - F_{pl,f}) + (F_c - F_{pl,c}) \cdot \tan\gamma}{(F_c - F_{pl,c}) + (F_f - F_{pl,f}) \cdot \tan\gamma} \quad (5)$$

with  $F_{pl,c}$  and  $F_{pl,f}$  being the ploughing force components exerted in normal and feed direction. The friction coefficient  $\mu_{fr}$  equals the slope in a  $F_f - F_c$  - plot where at higher feeds ploughing effects diminish since the ratio of the cutting edge radius  $r_n$  to the feed  $f$  becomes very small. Using the measured process forces of all Ti6Al4V-experiments, the trend in Figure 30 becomes visible from which the friction coefficient can be estimated as  $\mu_{fr} = 0.3$ . Similarly, for Ck45 the friction coefficient is about  $\mu_{fr} = 0.78$ , which is a very high value and most likely inaccurate due to changes in BUE-formation and chip segmentation. It is emphasized that a more credible deduction of friction coefficients requires cutting tests with specially prepared cutting edge radii  $r_n$  as for example used in [39]. Alternatively, in-process tribometer can be used for the determination of the friction coefficient [24] directly on the fresh cut surface.

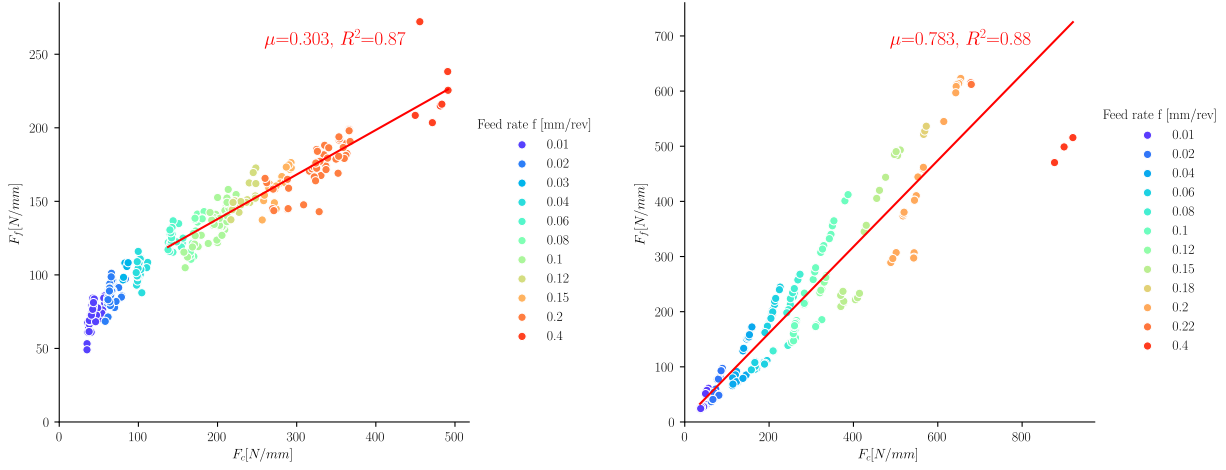


Figure 30: Friction coefficient  $\mu_{fr}$  estimation based on Albrecht [1] for Ti6Al4V (left) and Ck45 (right). The estimated friction coefficient for Ck45 is very high and most likely inaccurate due to changes in BUE-formation and chip segmentation.

### 3.5. Tempering Colours

During the cutting, the temperature in the chips increases due to plastic dissipation in the primary shear zone and friction in the secondary shear zone. In the case of the Ck45, these temperature increases lead to visible tempering colours in the chips, which can be matched to tabulated values [11]. The tempering colours can indicate temperatures as low as  $T_{min} = 200^\circ$  and as high as  $T_{max} = 360^\circ C$ . All Ck45 chips are manually analysed and the tempering colour dependence on the cutting speed is shown for selected feeds together with interpolated contour plots in Figure 31. At low cutting speeds, temperatures are in the order of the maximum temperature  $T_{max} = 360^\circ C$ . With increasing cutting speed the temperatures first reduces to levels below  $T = 300^\circ C$  between  $v_c = 100..200m/min$ . In cutting speed ranges of  $v_c \approx 200..450m/min$  the temperatures increase to  $T_{max} \approx 360^\circ$  followed by a temperature reduction when the cutting speed is increased beyond  $v_c \approx 450m/min$ . A possible explanation of this effect is a change in the chip formation mechanism see chapter 3.2 and Figure 25.

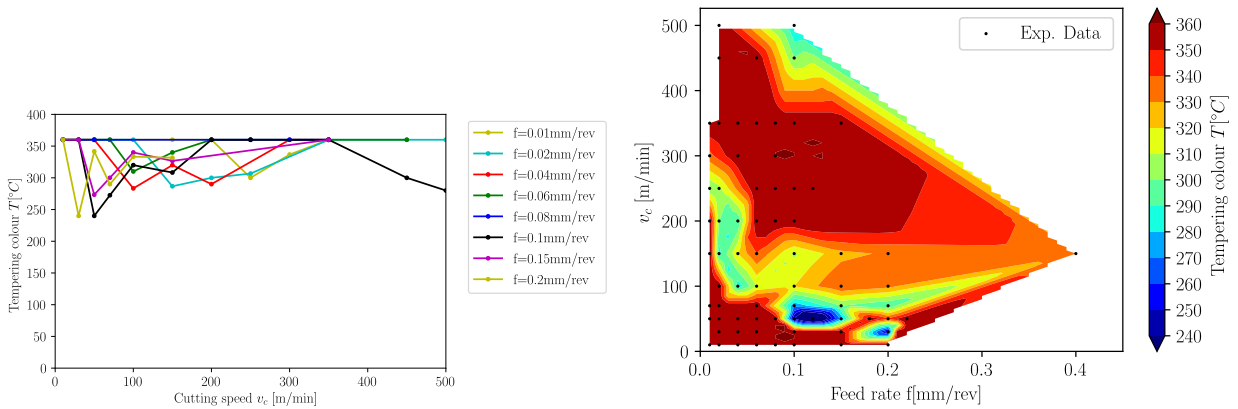


Figure 31: Estimated Ck45 chip temperatures based on tempering colours for different feeds  $f$  and varying cuttings speeds  $v_c$ . Evaluation for selected feeds (left) and interpolated contour plot (right) with black dots denoting the experimental data points which have been used for the interpolation.

### 3.6. Tool Wear

The tool wear depends on the feed, cutting speed and the amount of material removed at these parameters. For each cutting experiment the tool wear is visually inspected and qualitatively classified into three categories:

- Low (L): no or very few remains of material sticking to the rake and/or clearance face of the cutter
- Medium (M): beginning crater wear, material built-up on rake and/or clearance face
- High (H): heavy crater wear, cutting edge worn, large material built-up

Examples of different tool wear classifications are shown in 32. The tool wear classification is given for each experiment in the result tables B.14 (Ti6Al4V) and B.15 (Ck45).

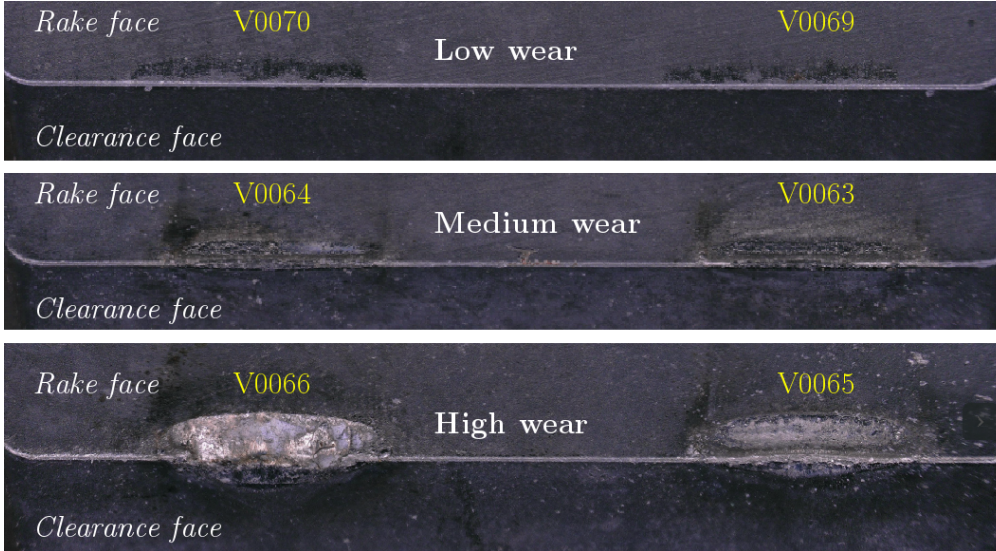


Figure 32: Wear classification of the cutter inserts: examples for low (top), medium (middle) and high (bottom) wear. The text in yellow colour depicts the corresponding experiment number.

### 3.7. Kienzle Coefficients

The Kienzle-Victor process force model [18] is an empirical equation that relates the cutting force  $F_c$  to the cut width  $b$ , uncut chip thickness  $h$  and a factor  $k_c$  which is the cutting force per unit area:

$$F_c = k_c \cdot a_p \cdot f = k_c \cdot b \cdot h \quad (6)$$

All effects of the process conditions like cutting speed, tool geometry as well as workpiece and tool material are contained in  $k_c$ . It was found by Kienzle that the cut width  $b$  scales linearly with the cutting force while the uncut chip thickness scales with a power law, where  $k_{c1.1}$  is the specific cutting force at  $b = h = 1$  mm:

$$F_c = k_{c1.1} \cdot h^{1-m_c} \quad (7)$$

The model can be extended to feed and passive force as well [22]:

$$F_f = k_{f1.1} \cdot h^{1-m_f} \quad (8)$$

$$F_p = k_{p1.1} \cdot h^{1-m_p} \quad (9)$$

In quasi-orthogonal cutting the passive force component is  $F_p \approx 0$  and therefore equations (7) and (8) are used to determine the Kienzle-coefficients  $k_{c1.1}(v_c)$ ,  $k_{f1.1}(v_c)$  and the respective exponents  $m_c(v_c)$ ,  $m_f(v_c)$  at different cutting speeds for Ti6Al4V and Ck45. For this purpose  $k_c$  and  $k_f$  are computed from the process forces and are extrapolated to  $f = 1\text{mm}$  for each cutting speed. Examples of such extrapolations are shown in Figure 33 for two different cutting speeds.

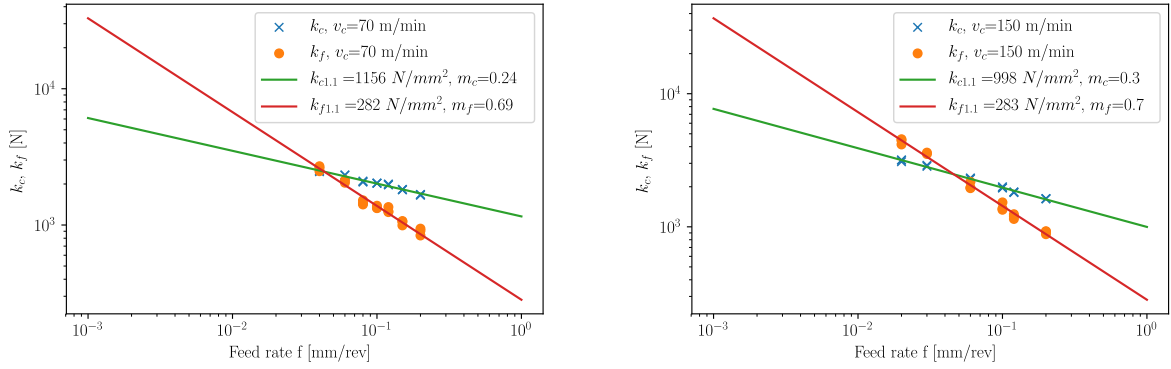


Figure 33: Kienzle coefficient determination for Ti6Al4V at cutting speeds of  $v_c = 70\text{m/min}$  (left) and  $v_c = 150\text{m/min}$  (right).

Figure 34 shows the dependencies of the Kienzle-coefficients on the cutting speed for Ti6Al4V. The corresponding values are supplied in table C.16 in the Appendix C. Towards higher cutting speeds the specific cutting and feed force coefficients reduce, while the exponents  $m_c, m_f$  increase.

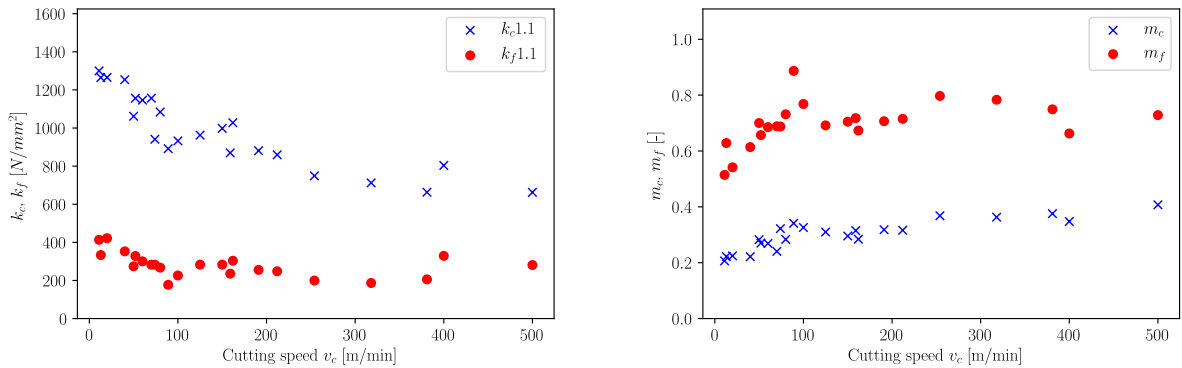


Figure 34: Kienzle coefficients for Ti6Al4V and various cutting speeds  $v_c$ .

For Ck45, the specific cutting and feed force coefficients slightly reduce until cutting speeds of  $v_c = 150\text{m}/\text{min}$ , followed by an increase towards  $v_c = 300\text{m}/\text{min}$  and reduce from thereon strongly. The increase around  $v_c = 300\text{m}/\text{min}$  is possibly induced by the dynamic strain aging (DSA) phenomenon [4, 5, 27]. Figure 35 shows the dependencies of the Kienzle-coefficients on the cutting speed for Ck45. The corresponding values are supplied in table C.17 in the Appendix C.

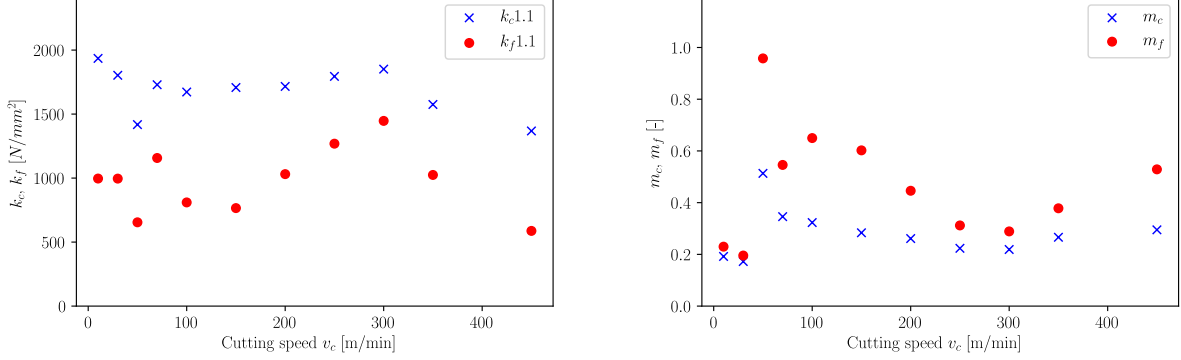


Figure 35: Kienzle coefficients for Ck45 and various cutting speeds  $v_c$ .

### 3.8. Data Storage

The data is stored in the [pCloud](#) and contains process force measurement data, cutting edge radii scans, pictures of chip geometries and etched chips, see the respective links in table 11.

Data	Saving location	Comment
Process forces	<a href="#">pCloud</a>	data format: time [s], $F_p$ [N/mm], $F_f$ [N/mm], $F_c$ [N/mm]
Cutting edge scans	<a href="#">pCloud</a>	new inserts, informations in CutPositionsOnCuttingEdge.xls
Chip images,	<a href="#">pCloud</a>	overview
Chip images (polished)	<a href="#">pCloud</a>	microscope images
Chip images (etched)	<a href="#">pCloud</a>	microscope images with chip microstructures

Table 11: Data storage of the quasi-orthogonal cutting experiments.

## 4. Conclusions

Large scale dry quasi-orthogonal cutting experiments have been conducted for Ti6Al4V and Ck45. Prior to the cutting tests a material characterization was conducted revealing:

- uniform hardness profiles in hardness measurements,
- uniform grain structures in etched samples,
- average grain diameters in the order of  $D_g \approx 9..10\mu\text{m}$  for Ti6Al4V and  $D_g \approx 14..18\mu\text{m}$  for Ck45 and
- yield strengths in the order of  $\sigma_y = 867\text{MPa}$  for Ti6Al4V and  $\sigma_y = 392\text{MPa}$  for Ck45.

Johnson-Cook flow stress model coefficients were given for the work hardening and strain rate sensitivity part, where the latter is valid only for very low strain rates. Since the tensile tests were conducted at room temperature, the temperature dependent part of the JC-law was not fitted.

Each cutting experiment was performed with a pristine cutting edge such that wear effects on the measured process forces could mostly be neglected. Since the cutting edge radius influences the process forces, every cutting edge was measured prior to the cutting tests, such that the average cutting edge radius could be retrieved at the respective cutting position.

For Ti6Al4V, the influence of the cutting edge radius on the measured process forces could be shown. Ploughing effects on the process forces were visible towards lower feeds. A friction coefficient of about  $\mu_{fr} \approx 0.3$  was estimated based on the process forces depending on the feed rates. Chip segmentations were found at all tested combinations of feeds and cutting speeds.

In the Ck45 cutting experiments a direct correlation of the cutting edge radius with the process forces is not visible. This is induced due to changing physics, e.g. dynamic strain aging, of the chip formation at different feeds and cutting speeds, where at lower values evidence for built-up edge formation was found on the chips and towards higher values chip segmentations occurred. The friction is not just depending on the feed, but also on the cutting speed where at medium cutting speeds the friction is higher than at very low and very high cutting speeds.

The measurement of chip thicknesses came along with scatter of the measured values, potential reasons for this scatter are:

- the manual measurement procedure,
- misalignments of chips in the embedding procedure because the chips are curled not only in feed direction but also due to the cylinder radius and
- low stiffness of thinner chips which could lead to skewing and therefore larger effective cross-sections after embedding.

The low stiffness of thinner chips prevented as well from the large scale evaluation of chip curling radii. Chip curling with the cylinder radius can be prevented by using a planing setup which is the best approximation to orthogonal cutting at the expense of lower maximum cutting speeds in the order of up to  $v_c = 30m/min$ .

## 5. Acknowledgements

The authors would hereby like to thank Adrian Fuhrer, Igor Podjanin, Knut Krieger, Matthias R othlin, Mohamadreza Afrasiabi, Fabian Kneub uhler, Moritz Wiessner, Mikhail Klyuev, Sandro Wigger, Albert Weber, Christoph Baumgart, Lukas Seeholzer, the IVP institute at ETH Z urich, Dr. Thomas Tancogne-Dejean (ETH) for the help with the EBSD images and the Swiss National Science Foundation (SNF) for the financial support under Grant No. 200021-149436.

## Appendix A. Test Overview

Tables [A.12](#) and [A.13](#) contain the cutting experiment numbers sorted according to feed (columns) and cutting speeds (rows) for Ti6Al4V and Ck45, respectively. The cutting experiment numbers can be used to find more information of the respective experiment in tables [B.14](#) and [B.15](#). The colouring of the experiment number indicates:

- black: no chip thickness measurement available,
- orange: chip thickness measurement available,
- green: chip thickness measurement and etched chip picture available.

$f$ [mm/rev] / $v_c$ [m/min]	0.01	0.02	0.03	0.04	0.06	0.08	0.1	0.12	0.15	0.2	0.4
10.0		V0301, V0302, V0303			V0304, V0305, V0306		V0307, V0308, V0309, V0319				
11.0	V0001, V0003, V0014						V0005, V0007, V0016, V0018			V0010, V0012, V0020	
13.0	V0002, V0013, V0015						V0004, V0006, V0008, V0009, V0017			V0011, V0019, V0021	
20.0	V0320, V0321, V0322	V0356, V0357, V0358		V0323, V0324, V0325	V0374, V0375, V0376, V0392	V0359, V0360, V0361	V0326, V0327, V0328	V0377, V0378, V0379	V0362, V0363, V0364	V0380, V0381, V0382	
40.0	V0338, V0339, V0340			V0341, V0342, V0343	V0480, V0481, V0482		V0344, V0345, V0346		V0483, V0484, V0485	V0486, V0487, V0488	
50.0		V0310, V0311, V0312		V0393, V0394, V0395	V0313, V0314, V0315	V0396, V0397, V0398	V0316, V0317, V0318		V0399, V0400, V0401	V0414, V0415, V0416	
52.0		V0417, V0418, V0419				V0420, V0421, V0422		V0423, V0424, V0425			
60.0		V0435, V0436, V0437, V0444, V0445					V0438, V0439, V0440			V0441, V0442, V0443	
70.0				V0402, V0403, V0404	V0383, V0384, V0385	V0405, V0406, V0407	V0411, V0412, V0413	V0386, V0387, V0388	V0408, V0409, V0410	V0389, V0390, V0391	
74.0	V0022, V0024						V0026			V0028, V0030	
80.0		V0446, V0453, V0454					V0447, V0448, V0449			V0450, V0451, V0452	
89.0	V0023						V0025, V0027			V0029	
100.0	V0329, V0330, V0331	V0365, V0366, V0367		V0332, V0333, V0334	V0498, V0499, V0500	V0368, V0369, V0370	V0335, V0336, V0337	V0501, V0502, V0503	V0371, V0372, V0373	V0504, V0505, V0506	
125.0	V0347, V0348, V0349			V0350, V0351, V0352	V0489, V0490, V0491		V0353, V0354, V0355		V0492, V0493, V0494	V0495, V0496, V0497	
150.0		V0516, V0517, V0518	V0519, V0520		V0507, V0508, V0509		V0455, V0456, V0457	V0510, V0511, V0512		V0513, V0514, V0515	
159.0	V0032						V0034			V0037, V0039	V0041
162.0		V0426, V0427, V0428				V0429, V0430, V0431		V0432, V0433, V0434			
191.0	V0031, V0033						V0035			V0038	V0040, V0042
200.0							V0458, V0459, V0460				
212.0	V0043, V0045						V0047, V0049			V0051	V0053, V0055
254.0	V0044, V0046						V0048			V0050, V0052, V0068	V0054
318.0	V0057						V0059, V0061			V0063	V0065, V0067
381.0	V0056, V0058						V0060			V0062, V0064	V0066
400.0	V0461, V0462, V0463	V0464, V0465, V0466	V0467, V0468, V0469	V0470, V0471, V0472							
500.0	V0473, V0474, V0475	V0476, V0477, V0478					V0479				

Table A.12: Ti6Al4V: Overview of process parameter combinations and according test numbers.

$f[mm/rev]$ / $v_c[m/min]$	0.01	0.02	0.04	0.06	0.08	0.1	0.12	0.15	0.18	0.2	0.22	0.4	1.0
10.0	V0069, V0070, V0071, V0212, V0213, V0214	V0176, V0177, V0178	V0215, V0216, V0217	V0179, V0180, V0181	V0218, V0219, V0220	V0072, V0073, V0074		V0182, V0183, V0184		V0075, V0076, V0077, V0078			
30.0		V0102, V0103, V0104	V0120, V0121, V0122	V0105, V0106, V0107		V0123, V0124, V0125		V0108, V0109, V0110		V0126, V0127, V0128			V0138
50.0	V0252, V0253, V0254	V0139, V0140, V0141	V0157, V0158, V0159	V0142, V0143, V0144	V0255, V0256, V0257	V0160, V0161, V0162	V0258, V0259, V0260	V0145, V0146, V0147	V0270, V0271, V0272, V0273	V0163, V0164, V0165, V0295, V0296, V0297	V0274, V0275, V0276		
70.0	V0079, V0080, V0081	V0185, V0186, V0187		V0188, V0189, V0190		V0082, V0083, V0084, V0085		V0191, V0192, V0193		V0086, V0087, V0088, V0089			
100.0		V0111, V0112, V0113	V0129, V0130, V0131	V0114, V0115, V0116		V0132, V0133, V0134		V0117, V0118, V0119		V0135, V0136, V0137			
150.0	V0090, V0091, V0092	V0148, V0149, V0150, V0175	V0166, V0167, V0168	V0151, V0152, V0153		V0093, V0094, V0095, V0169, V0170, V0171		V0154, V0155, V0156		V0096, V0097, V0098, V0172, V0173, V0174		V0099, V0100, V0101	
200.0	V0194, V0195, V0196	V0277, V0278, V0279	V0197, V0198, V0199	V0280, V0281, V0282	V0200, V0201, V0202	V0283, V0284, V0285							
250.0	V0261, V0262, V0263	V0230, V0231, V0232		V0233, V0234, V0235	V0264, V0265, V0266	V0236, V0237, V0238	V0267, V0268, V0269						
300.0	V0203, V0204, V0205		V0206, V0207, V0208		V0209, V0210, V0211								
350.0	V0221, V0222, V0223	V0239, V0240, V0241	V0224, V0225, V0226	V0242, V0243, V0244	V0227, V0228, V0229	V0245, V0246, V0247		V0248, V0249, V0250					
450.0		V0286, V0287, V0288		V0289, V0290, V0291		V0292, V0293, V0294							
500.0		V0251				V0298, V0299, V0300							

Table A.13: Ck45: Overview of process parameter combinations and according test numbers.

## Appendix B. Experimental Results

The complete cutting test results are provided for Ti6Al4V (V0001-V0068, V0301-V0520) in table B.14 and for Ck45 (V0069-V0300) in table B.15 below. Blue coloured experiment numbers contain a link to a high-speed camera video of that test. The process forces  $F_c$  and  $F_f$  are normalized to a cutting width of  $w = 1\text{mm}$  and are given together with their respective standard deviations  $\sigma_{F_c}$  and  $\sigma_{F_f}$ . The next two columns contain the averaged cutting edge radius  $r_n$  and its standard deviation  $\sigma_{r_n}$ , followed by the average chip thickness  $h_{avg}$  and its standard deviation  $\sigma_{h_{avg}}$  (if more than one chip is evaluated), the cutting distance  $l_{cut}$  and the temperature of the chip  $T_{chip}$  derived from the tempering color (only Ck45). The last two columns contain a qualitative statement of the tool wear and STATUS judges the quality of the process forces measurement. Tests labelled with **ok** are without any objections. Tests labelled **short** have to be treated with care as such experiments should be repeated with a longer cutting distance in order for the process forces to reach a stable value. If however the standard deviations in the process forces of such tests are small, they still can be considered as valid. Results from tests labelled **questionable** or **initially stable** should not be used for parameter identifications while tests labelled with **saturation** ran into the amplifier limits and are therefore invalid for further use. Tests marked **instable** are most likely of insufficient quality and must not be used for parameter identifications as well. Nonetheless, invalid experiments are listed in the results tables for two reasons. First, critical process parameters are known then. Second, the generated chips can be still used for evaluation at these process conditions.

Test	$v_c$ [m/min]	$f$ [mm/rev]	$F_c$ [N]	$\sigma_{F_c}$ [N]	$F_f$ [N]	$\sigma_{F_f}$ [N]	$r_n$ [ $\mu\text{m}$ ]	$\sigma_{r_n}$ [ $\mu\text{m}$ ]	$h_{avg}$ [ $\mu\text{m}$ ]	$\sigma_{h_{avg}}$ [ $\mu\text{m}$ ]	$l_{cut}$ [mm]	$T_{chip}$ [K]	Wear	Status
V0001	10.5	0.01	55.7	2.1	83.8	4.9	37.1	2.0	34.4	9.1	2024	-	L	ok
V0002	12.6	0.01	55.2	1.8	76.4	4.2	32.0	2.4	38.3	8.3	2024	-	L	ok
V0003	10.5	0.01	57.4	1.8	80.7	4.6	30.8	4.0	44.0	20.8	2024	-	L	ok
V0004	12.6	0.1	214.0	7.7	149.0	6.5	33.5	3.2	160.4	-	607	-	L	ok
V0005	10.5	0.1	209.1	7.0	130.7	5.2	27.4	5.0	158.4	-	607	-	L	ok
V0006	12.6	0.1	210.4	7.0	138.1	6.0	29.8	2.1	130.8	33.2	607	-	L	ok
V0007	10.5	0.1	0.0	0.0	0.0	0.0	33.8	2.2	175.4	-	607	-	M	error
V0008	12.6	0.1	0.0	0.0	0.0	0.0	30.3	1.9	358.1	19.2	607	-	L	error
V0009	12.6	0.1	0.0	0.0	0.0	0.0	30.3	1.9	157.7	-	607	-	L	error
V0010	10.5	0.2	361.3	15.3	189.1	7.1	31.4	2.4	279.4	-	607	-	L	ok
V0011	12.6	0.2	363.5	14.2	182.5	6.2	28.1	5.7	279.4	-	607	-	L	ok
V0012	10.5	0.2	366.1	14.5	199.1	7.4	31.7	2.9	341.8	-	607	-	L	ok
V0013	12.6	0.01	54.9	1.8	76.2	4.4	32.0	4.1	31.1	2.2	2024	-	L	ok
V0014	10.5	0.01	53.3	1.6	70.2	3.8	25.4	3.3	29.8	-	2024	-	L	ok
V0015	12.6	0.01	53.8	1.6	74.0	4.0	31.6	4.0	32.1	1.4	2024	-	L	ok
V0016	10.5	0.1	207.0	6.6	132.8	5.0	28.9	3.9	219.3	73.5	607	-	L	ok
V0017	12.6	0.1	208.0	7.2	138.3	5.6	31.3	2.1	180.0	0.5	607	-	L	ok
V0018	10.5	0.1	211.4	7.2	141.6	6.2	31.9	2.0	211.2	55.6	607	-	L	ok
V0019	12.6	0.2	362.2	13.9	181.2	6.4	26.2	3.1	288.1	-	607	-	L	ok
V0020	10.5	0.2	360.2	12.0	179.2	5.6	25.2	3.8	385.7	40.0	607	-	L	ok
V0021	12.6	0.2	358.8	12.8	186.6	6.7	30.5	2.1	296.6	42.1	607	-	L	ok
V0022	74.3	0.01	40.3	1.2	61.0	2.7	27.2	3.3	22.3	-	2024	-	L	ok
V0023	88.9	0.01	0.0	0.0	0.0	0.0	30.8	2.7	22.4	0.3	2024	-	L	error
V0024	74.3	0.01	42.7	1.3	73.2	3.3	34.2	2.9	24.1	2.7	2024	-	L	ok
V0025	88.9	0.1	194.8	5.4	133.6	3.8	31.3	2.8	126.7	0.9	607	-	L	short
V0026	74.3	0.1	195.9	5.3	137.5	4.6	33.6	5.3	113.6	6.9	607	-	L	short
V0027	88.9	0.1	196.3	4.2	139.4	3.3	30.8	2.5	139.2	18.3	607	-	L	short
V0028	74.3	0.2	316.1	9.1	170.5	3.8	32.0	1.9	202.5	24.2	607	-	L	short
V0029	88.9	0.2	308.8	4.5	147.6	2.3	27.1	4.0	202.7	6.5	607	-	L	short
V0030	74.3	0.2	319.2	6.7	172.1	3.3	33.3	1.8	232.9	33.3	607	-	L	short
V0031	190.5	0.01	35.1	0.7	53.2	1.1	23.8	1.9	18.0	2.2	2024	-	L	ok
V0032	159.1	0.01	37.1	1.0	64.2	1.4	29.1	2.9	25.7	-	2024	-	L	ok
V0033	190.5	0.01	41.3	0.7	79.2	1.3	34.2	1.7	18.4	-	2024	-	L	ok
V0034	159.1	0.1	179.4	4.6	126.9	2.2	33.6	2.4	113.5	-	607	-	L	short
V0035	190.5	0.1	175.5	1.4	119.2	0.8	32.7	1.8	148.9	25.9	607	-	L	short
V0037	159.1	0.2	288.5	6.2	144.5	2.8	29.7	4.0	206.8	9.4	607	-	M	short
V0038	190.5	0.2	289.8	4.8	158.9	2.4	32.8	2.2	198.0	-	607	-	M	short
V0039	159.1	0.2	289.2	3.3	145.0	2.2	29.3	3.6	198.8	-	607	-	M	short
V0040	190.5	0.4	491.3	7.5	225.5	9.3	28.9	4.2	337.1	-	607	-	M	short
V0041	159.1	0.4	471.4	16.9	203.5	19.6	33.3	2.9	365.6	-	607	-	M	short
V0042	190.5	0.4	490.8	8.5	238.2	8.3	35.6	2.4	368.6	-	607	-	M	short
V0043	212.2	0.01	36.0	1.1	67.5	1.4	30.0	4.3	19.2	-	2024	-	L	ok
V0044	254.1	0.01	42.3	0.8	84.2	1.5	37.5	1.7	17.6	-	4049	-	L	ok
V0045	212.2	0.01	38.0	0.9	66.4	1.5	30.5	2.0	24.3	-	4049	-	L	ok
V0046	254.1	0.01	39.5	0.8	72.5	1.2	32.1	3.6	19.6	2.8	4049	-	L	ok
V0047	212.2	0.1	171.0	2.3	120.9	1.0	33.8	2.8	117.3	10.7	607	-	L	short
V0048	254.1	0.1	168.3	2.3	119.0	1.9	32.9	2.5	87.9	3.3	607	-	L	short
V0049	212.2	0.1	171.8	2.8	126.7	2.0	36.8	1.9	85.0	-	607	-	L	short
V0050	254.1	0.2	269.5	4.1	145.0	2.9	31.4	2.1	146.2	1.8	607	-	L	short
V0051	212.2	0.2	288.3	6.1	165.0	4.4	37.5	2.1	201.3	6.8	607	-	L	short
V0052	254.1	0.2	271.2	7.1	143.7	4.7	31.3	2.8	166.6	35.4	607	-	L	short
V0053	212.2	0.4	481.5	13.6	214.9	5.9	31.7	2.3	298.5	12.1	607	-	M	short

Test	$v_c$ [m/min]	$f$ [mm/rev]	$F_c$ [N]	$\sigma_{F_c}$ [N]	$F_f$ [N]	$\sigma_{F_f}$ [N]	$r_n$ [ $\mu$ m]	$\sigma_{r_n}$ [ $\mu$ m]	$h_{avg}$ [ $\mu$ m]	$\sigma_{h_{avg}}$ [ $\mu$ m]	$l_{cut}$ [mm]	$T_{chip}$ [K]	Wear	Status
V0054	254.1	0.4	449.8	12.2	208.4	7.9	35.3	3.4	234.9	17.2	607	-	M	short
V0055	212.2	0.4	483.4	8.0	216.1	4.1	33.4	3.7	351.4	38.0	607	-	M	short
V0056	381.3	0.01	38.6	0.7	68.6	1.2	33.0	3.0	20.4	1.9	4049	-	L	ok
V0057	318.5	0.01	38.0	0.8	69.0	1.2	34.2	2.2	14.0	-	4049	-	L	ok
V0058	381.3	0.01	36.2	0.7	61.0	1.0	28.4	2.3	18.3	-	4049	-	L	ok
V0059	318.5	0.1	162.0	3.5	112.1	2.6	32.2	2.2	223.9	101.9	1214	-	L	short
V0060	381.3	0.1	157.5	3.3	115.5	2.8	33.0	2.4	99.7	-	1214	-	L	short
V0061	318.5	0.1	159.1	3.8	104.9	3.0	28.7	4.6	122.3	10.1	1214	-	L	short
V0062	381.3	0.2	262.1	5.7	162.7	11.8	34.1	2.1	145.4	6.5	1214	-	M	short
V0063	318.5	0.2	270.3	4.9	158.3	6.0	32.5	2.1	147.7	10.1	1214	-	M	short
V0064	381.3	0.2	260.0	4.3	165.6	9.5	35.2	2.7	153.5	-	1214	-	M	short
V0065	318.5	0.4	455.6	10.5	272.1	32.2	36.8	2.2	232.3	20.9	1214	-	H	short
V0066	381.3	0.4	468.5	9.4	412.3	59.6	34.8	2.1	161.5	-	1214	-	H	error
V0067	318.5	0.4	453.9	12.1	253.6	28.6	35.8	4.2	261.3	-	1214	-	H	error
V0068	254.1	0.2	299.5	12.7	305.9	103.5	29.8	5.0	212.3	2.5	11136	-	H	error
V0301	10.0	0.02	79.0	2.3	85.7	5.3	36.8	3.0	-	-	3324	-	L	ok
V0302	10.0	0.02	83.5	2.4	97.2	5.9	41.2	2.2	93.1	27.3	3324	-	L	ok
V0303	10.0	0.02	78.5	2.2	84.9	5.3	34.1	2.8	-	-	3324	-	L	ok
V0304	10.0	0.06	155.4	4.8	121.7	6.5	40.6	2.4	103.6	6.8	3324	-	L	ok
V0305	10.0	0.06	154.3	4.9	118.9	6.5	39.9	2.9	-	-	3324	-	L	ok
V0306	10.0	0.06	156.4	5.0	125.0	6.9	41.3	2.5	-	-	3324	-	L	ok
V0307	10.0	0.1	-0.2	2.3	-0.1	1.4	34.4	4.3	-	-	3324	-	L	error
V0308	10.0	0.1	223.0	7.2	152.4	7.7	42.2	4.4	-	-	3324	-	L	ok
V0309	10.0	0.1	223.5	7.8	154.6	8.4	42.4	3.6	164.2	4.2	3324	-	L	ok
V0310	50.1	0.02	61.7	1.7	71.4	3.3	32.4	4.0	-	-	3324	-	L	ok
V0311	50.1	0.02	68.2	1.9	95.1	4.7	42.5	1.9	49.3	7.9	3324	-	L	ok
V0312	50.1	0.02	67.1	1.8	89.8	4.4	40.7	2.4	-	-	3324	-	L	ok
V0313	50.1	0.06	139.8	4.2	121.3	4.5	38.4	2.9	-	-	3324	-	L	ok
V0314	50.1	0.06	141.5	4.4	126.7	4.7	40.2	3.6	-	-	3324	-	L	ok
V0315	50.1	0.06	138.4	4.2	117.8	4.4	38.3	2.7	75.7	3.6	3324	-	L	ok
V0316	50.1	0.1	211.4	6.2	143.2	3.7	38.7	2.5	-	-	3324	-	L	ok
V0317	50.1	0.1	210.8	6.2	141.6	3.8	36.7	2.2	-	-	3324	-	L	ok
V0318	50.1	0.1	210.9	5.9	140.6	3.4	36.3	2.2	152.1	-	3324	-	L	ok
V0319	10.0	0.1	221.9	7.1	145.8	7.1	37.7	2.4	-	-	3324	-	L	ok
V0320	19.9	0.01	55.9	3.1	84.5	5.2	40.5	2.8	22.8	-	3324	-	L	ok
V0321	19.9	0.01	57.2	1.8	85.8	5.1	39.2	2.3	-	-	3324	-	L	ok
V0322	19.9	0.01	56.2	2.2	84.3	5.0	39.5	2.2	-	-	3324	-	L	ok
V0323	19.9	0.04	111.7	4.2	108.5	5.9	38.1	3.1	-	-	3324	-	L	ok
V0324	19.9	0.04	104.3	3.1	87.8	4.4	31.2	3.6	-	-	3324	-	L	ok
V0325	19.9	0.04	110.5	3.5	104.9	5.6	37.5	2.6	74.5	10.7	3324	-	L	ok
V0326	19.9	0.1	211.1	6.5	146.8	6.4	37.3	2.0	-	-	3324	-	M	ok
V0327	19.9	0.1	213.5	6.8	158.1	7.1	42.9	2.2	-	-	3324	-	M	ok
V0328	19.9	0.1	205.8	6.4	133.0	5.5	33.5	3.5	146.7	-	3324	-	M	ok
V0329	100.0	0.01	44.1	1.0	81.4	3.3	40.6	2.1	-	-	3324	-	L	ok
V0330	100.0	0.01	43.5	1.1	77.7	3.1	40.0	2.7	-	-	3324	-	L	ok
V0331	100.0	0.01	43.6	1.0	78.7	3.1	38.8	2.7	22.8	1.1	3324	-	L	ok
V0332	100.0	0.04	99.0	2.1	96.0	2.4	33.8	3.3	-	-	3324	-	L	ok
V0333	100.0	0.04	98.4	2.0	93.9	2.1	34.5	3.2	73.4	13.7	3324	-	L	ok
V0334	100.0	0.04	102.8	2.4	111.5	3.0	41.0	2.7	-	-	3324	-	L	ok
V0335	100.0	0.1	203.3	2.9	140.0	2.3	37.9	4.7	-	-	3324	-	M	ok
V0336	100.0	0.1	200.0	2.3	122.0	1.5	32.5	3.6	180.3	-	3324	-	M	ok
V0337	100.0	0.1	199.2	2.5	123.6	2.0	32.8	3.2	-	-	3324	-	M	ok
V0338	39.9	0.01	48.5	1.3	77.5	3.9	42.4	2.2	-	-	3324	-	L	ok
V0339	39.9	0.01	47.1	1.2	72.6	3.8	39.1	4.8	-	-	3324	-	L	ok
V0340	39.9	0.01	45.9	1.2	68.2	3.6	35.2	2.4	24.7	2.7	3324	-	L	ok
V0341	39.9	0.04	102.3	3.0	100.2	4.6	36.7	2.4	-	-	3324	-	L	ok
V0342	39.9	0.04	103.1	3.0	103.7	4.9	38.0	2.4	-	-	3324	-	L	ok
V0343	39.9	0.04	100.3	2.9	97.7	4.4	36.0	4.4	87.3	33.7	3324	-	L	ok
V0344	39.9	0.1	211.9	6.8	152.2	5.1	40.1	3.2	-	-	3324	-	L	ok
V0345	39.9	0.1	209.0	6.6	143.5	4.4	37.4	2.3	-	-	3324	-	L	ok
V0346	39.9	0.1	209.3	6.8	143.8	4.9	36.7	2.1	133.4	-	3324	-	L	ok
V0347	125.0	0.01	35.0	0.7	49.1	1.5	28.6	4.1	-	-	3324	-	L	ok
V0348	125.0	0.01	42.7	0.9	77.5	2.6	38.3	2.4	19.4	-	3324	-	L	ok
V0349	125.0	0.01	43.1	0.9	78.8	2.6	38.9	2.3	-	-	3324	-	L	ok
V0350	125.0	0.04	102.3	2.3	110.9	3.2	37.9	2.4	62.4	-	3324	-	L	ok
V0351	125.0	0.04	97.7	2.2	93.0	2.5	32.9	2.6	-	-	3324	-	L	ok
V0352	125.0	0.04	101.5	2.3	107.1	3.0	39.5	4.2	-	-	3324	-	L	ok
V0353	125.0	0.1	197.3	2.1	141.2	1.7	40.5	3.0	192.0	47.7	3324	-	M	ok
V0354	125.0	0.1	197.7	2.0	141.2	1.8	40.1	3.1	-	-	3324	-	M	ok
V0355	125.0	0.1	195.9	2.0	138.9	1.7	39.8	2.4	-	-	3324	-	M	ok
V0356	19.9	0.02	69.9	1.9	77.8	4.2	36.1	2.8	-	-	3324	-	L	ok
V0357	19.9	0.02	75.1	2.0	91.4	5.1	40.9	2.1	-	-	3324	-	L	ok
V0358	19.9	0.02	71.8	1.9	82.0	4.5	35.4	2.0	45.6	13.3	3324	-	L	ok
V0359	19.9	0.08	170.1	5.1	112.5	4.4	30.7	3.3	-	-	3324	-	L	ok
V0360	19.9	0.08	174.4	5.4	127.9	6.0	38.8	2.8	124.7	-	3324	-	L	ok
V0361	19.9	0.08	177.0	5.6	138.3	6.6	42.5	2.4	-	-	3324	-	L	ok
V0362	19.9	0.15	291.4	9.5	171.8	5.9	38.5	2.7	-	-	3324	-	L	ok
V0363	19.9	0.15	292.8	9.7	176.4	6.1	39.2	2.3	211.6	-	3324	-	L	ok
V0364	19.9	0.15	293.2	9.4	172.8	5.5	38.4	3.2	-	-	3324	-	L	ok
V0365	100.0	0.02	61.0	1.4	80.6	3.0	37.2	2.8	39.4	14.1	3324	-	L	ok
V0366	100.0	0.02	62.9	1.5	89.9	3.2	37.5	3.0	-	-	3324	-	L	ok
V0367	100.0	0.02	60.9	1.3	82.5	3.0	35.0	3.1	-	-	3324	-	L	ok
V0368	100.0	0.08	173.8	3.3	129.3	2.8	39.2	3.4	111.2	5.1	3324	-	M	ok
V0369	100.0	0.08	175.4	3.1	137.6	2.6	42.5	3.5	-	-	3324	-	M	ok
V0370	100.0	0.08	174.7	3.2	135.9	2.7	44.6	7.2	-	-	3324	-	M	ok
V0371	100.0	0.15	265.0	3.0	161.1	2.1	43.3	4.0	-	-	3324	-	M	ok
V0372	100.0	0.15	265.7	3.0	161.8	2.2	42.6	3.2	-	-	3324	-	M	ok
V0373	100.0	0.15	264.8	3.0	159.1	2.0	41.1	3.0	315.8	86.7	3324	-	M	ok
V0374	19.9	0.06	148.2	4.4	122.5	5.6	34.5	2.6	121.5	28.7	3282	-	L	ok
V0375	19.9	0.06	150.9	4.5	134.9	6.7	40.7	2.1	-	-	3282	-	L	ok
V0376	19.9	0.06	143.6	4.3	115.4	5.1	32.4	3.1	-	-	3282	-	L	ok
V0377	19.9	0.12	248.4	7.8	172.7	6.2	40.4	2.2	164.5	10.0	3282	-	M	ok
V0378	19.9	0.12	240.7	7.3	149.2	4.5	33.0	4.2	-	-	3282	-	M	ok
V0379	19.9	0.12	245.1	7.8	169.6	6.3	40.7	2.7	-	-	3282	-	M	ok
V0380	19.9	0.2	366.6	14.0	198.7	9.1	40.9	2.8	237.1	20.2	3282	-	M	ok
V0381	19.9	0.2	366.3	13.4	198.0	9.8	37.8	2.1	-	-	3282	-	M	ok
V0382	19.9	0.2	367.6	13.6	190.7	9.5	36.5	3.0	287.4	76.1	3282	-	M	ok
V0383	70.0	0.06	140.0	3.7	127.8	3.3	41.6	2.2	99.9	17.0	3282	-	L	ok
V0384	70.0	0.06	-7.8	29.5	-11.									

Test	$v_c$ [m/min]	$f$ [mm/rev]	$F_c$ [N]	$\sigma_{F_c}$ [N]	$F_f$ [N]	$\sigma_{F_f}$ [N]	$r_n$ [μm]	$\sigma_{r_n}$ [μm]	$h_{avg}$ [μm]	$\sigma_{h_{avg}}$ [μm]	$l_{cut}$ [mm]	$T_{chip}$ [K]	Wear	Status
V0385	70.0	0.06	139.1	3.2	122.6	2.9	39.4	3.3	-	-	3282	-	L	ok
V0386	70.0	0.12	237.6	4.0	151.1	4.0	39.4	2.4	330.1	19.4	3282	-	M	ok
V0387	70.0	0.12	236.2	4.3	149.3	4.4	38.2	2.8	-	-	3282	-	M	ok
V0388	70.0	0.12	240.0	4.0	162.5	3.9	43.9	2.6	-	-	3282	-	M	ok
V0389	70.0	0.2	330.7	4.2	167.6	3.3	37.9	3.4	-	-	3282	-	M	ok
V0390	70.0	0.2	334.4	4.8	181.7	5.8	40.5	2.4	230.3	18.6	3282	-	M	ok
V0391	70.0	0.2	335.3	4.1	188.1	3.7	41.9	2.0	-	-	3282	-	M	ok
V0392	19.9	0.06	137.7	3.1	122.0	3.0	39.3	2.4	-	-	3282	-	L	ok
V0393	50.1	0.04	99.0	2.4	95.8	3.5	34.6	3.5	-	-	3282	-	L	ok
V0394	50.1	0.04	99.3	2.4	98.8	3.6	36.0	2.8	67.9	-	3282	-	L	ok
V0395	50.1	0.04	101.3	2.4	107.4	4.0	40.8	3.2	-	-	3282	-	L	ok
V0396	50.1	0.08	172.2	4.6	129.9	3.5	38.4	3.8	-	-	3282	-	L	ok
V0397	50.1	0.08	174.5	4.5	141.3	3.8	42.2	2.5	108.7	-	3282	-	L	ok
V0398	50.1	0.08	166.4	4.6	110.6	3.1	32.4	3.4	-	-	3282	-	L	ok
V0399	50.1	0.15	281.3	2.7	166.9	2.7	41.7	2.3	-	-	3282	-	M	ok
V0400	50.1	0.15	279.3	2.9	162.5	3.3	40.8	2.6	177.6	-	3282	-	M	ok
V0401	50.1	0.15	274.1	2.9	144.9	2.9	34.9	3.3	-	-	3282	-	M	ok
V0402	70.0	0.04	100.6	2.5	108.0	3.6	40.5	2.5	64.2	2.5	3282	-	L	ok
V0403	70.0	0.04	99.6	2.4	104.4	3.4	37.7	2.4	-	-	3282	-	L	ok
V0404	70.0	0.04	98.4	2.2	99.3	3.0	36.2	2.8	-	-	3282	-	L	ok
V0405	70.0	0.08	168.2	3.5	121.4	2.3	36.6	2.7	110.5	10.9	3282	-	M	ok
V0406	70.0	0.08	165.7	3.3	113.2	1.8	33.9	3.0	-	-	3282	-	M	ok
V0407	70.0	0.08	165.7	3.5	115.7	2.2	35.9	2.9	-	-	3282	-	M	ok
V0408	70.0	0.15	271.8	2.9	149.0	2.2	33.7	4.3	-	-	3282	-	M	ok
V0409	70.0	0.15	272.6	3.5	158.4	2.8	37.3	2.5	-	-	3282	-	M	ok
V0410	70.0	0.15	274.1	3.3	160.4	2.6	37.6	2.4	225.8	19.1	3282	-	M	ok
V0411	70.0	0.1	202.7	4.2	133.0	3.4	36.8	3.0	-	-	3282	-	M	ok
V0412	70.0	0.1	202.7	4.3	133.7	3.4	38.1	3.1	129.0	4.2	3282	-	M	ok
V0413	70.0	0.1	203.0	4.3	138.5	3.7	38.6	2.3	-	-	3282	-	M	ok
V0414	50.1	0.2	337.4	5.8	174.0	6.1	38.5	2.8	445.6	162.9	3282	-	M	ok
V0415	50.1	0.2	328.4	5.5	143.0	4.3	29.1	4.1	-	-	3282	-	M	ok
V0416	50.1	0.2	336.8	6.3	174.0	5.5	37.6	2.5	-	-	3282	-	M	ok
V0417	52.0	0.02	67.8	1.5	89.3	3.7	37.3	2.5	-	-	3435	-	L	ok
V0418	52.0	0.02	64.6	1.5	79.1	3.2	36.1	2.9	-	-	3435	-	L	ok
V0419	52.0	0.02	67.3	1.5	89.0	3.6	39.1	2.4	41.0	1.5	3435	-	L	ok
V0420	52.0	0.08	183.0	4.5	143.0	3.7	39.5	2.3	121.1	32.4	3435	-	L	ok
V0421	52.0	0.08	180.6	4.5	138.5	3.5	38.1	2.2	-	-	3435	-	L	ok
V0422	52.0	0.08	180.7	4.3	138.1	3.4	37.8	1.9	-	-	3435	-	L	ok
V0423	52.0	0.12	247.7	4.7	153.7	2.8	38.9	2.8	184.6	37.6	3435	-	L	ok
V0424	52.0	0.12	247.9	4.6	152.1	2.7	38.8	4.0	-	-	3435	-	L	ok
V0425	52.0	0.12	248.4	4.7	162.1	3.2	41.1	2.6	-	-	3435	-	L	ok
V0426	162.4	0.02	65.9	0.9	98.2	1.7	41.9	2.2	-	-	3435	-	L	ok
V0427	162.4	0.02	63.1	0.9	86.9	1.5	37.8	3.2	35.2	2.2	3435	-	L	ok
V0428	162.4	0.02	58.1	0.7	68.4	1.1	30.5	4.3	-	-	3435	-	L	ok
V0429	162.4	0.08	171.5	1.6	137.6	2.2	39.6	2.4	119.0	15.0	3435	-	M	ok
V0430	162.4	0.08	169.4	1.3	128.1	1.5	37.7	3.0	-	-	3435	-	M	ok
V0431	162.4	0.08	171.5	1.6	138.5	2.3	41.0	1.9	-	-	3435	-	M	ok
V0432	162.4	0.12	222.3	1.9	146.5	2.3	38.1	2.8	-	-	3435	-	M	ok
V0433	162.4	0.12	222.6	2.4	150.6	3.0	39.4	2.3	151.1	4.7	3435	-	M	ok
V0434	162.4	0.12	221.7	2.0	150.3	2.6	42.0	2.2	-	-	3435	-	M	ok
V0435	60.0	0.02	65.4	1.4	86.1	3.4	36.6	2.4	-	-	3435	-	L	ok
V0436	60.0	0.02	63.8	1.3	81.7	3.1	36.6	3.1	-	-	3435	-	L	ok
V0437	60.0	0.02	66.3	1.4	88.9	3.5	39.0	2.6	39.5	-	3435	-	L	ok
V0438	60.0	0.1	211.8	3.6	136.2	2.3	37.3	3.1	-	-	3435	-	M	ok
V0439	60.0	0.1	212.3	3.7	140.0	2.3	37.2	2.1	-	-	3435	-	M	ok
V0440	60.0	0.1	214.3	3.7	145.3	2.7	39.8	2.9	117.3	-	3435	-	M	ok
V0441	60.0	0.2	353.5	5.6	191.6	5.3	40.4	3.2	-	-	3435	-	M	ok
V0442	60.0	0.2	354.2	5.6	192.5	3.9	39.9	3.0	285.5	71.6	3435	-	M	ok
V0443	60.0	0.2	353.4	5.5	193.8	3.1	39.4	2.7	-	-	3435	-	M	ok
V0444	60.0	0.02	65.0	1.3	86.3	3.4	39.9	6.3	-	-	3435	-	L	ok
V0445	60.0	0.02	67.8	1.4	96.3	3.9	41.3	2.0	37.6	3.8	3435	-	L	ok
V0446	79.9	0.02	66.5	1.4	95.8	3.5	41.2	2.4	-	-	3435	-	L	ok
V0447	79.9	0.1	205.6	3.6	126.9	3.7	32.8	3.9	-	-	3435	-	M	ok
V0448	79.9	0.1	213.0	3.4	148.4	3.6	39.5	3.0	181.6	49.5	3435	-	M	ok
V0449	79.9	0.1	212.0	3.4	149.3	3.7	41.1	3.7	-	-	3435	-	M	ok
V0450	79.9	0.2	337.1	4.0	171.6	2.1	37.7	3.4	-	-	3435	-	M	ok
V0451	79.9	0.2	340.5	4.6	186.4	2.9	41.8	2.8	-	-	3435	-	M	ok
V0452	79.9	0.2	339.0	4.0	179.4	2.4	38.9	2.1	222.4	9.3	3435	-	M	ok
V0453	79.9	0.02	64.0	1.4	88.2	3.2	36.6	2.8	-	-	3435	-	L	ok
V0454	79.9	0.02	66.4	1.4	96.5	3.5	40.8	2.6	39.5	8.6	3435	-	L	ok
V0455	150.0	0.1	196.3	1.4	137.2	1.3	38.5	2.9	141.2	15.0	3435	-	M	ok
V0456	150.0	0.1	195.9	1.8	134.3	1.5	36.4	2.3	-	-	3435	-	M	ok
V0457	150.0	0.1	200.1	1.6	152.6	1.7	42.9	2.9	-	-	3435	-	M	ok
V0458	199.9	0.1	192.7	1.6	137.2	2.8	38.2	2.8	-	-	3435	-	M	short
V0459	199.9	0.1	190.5	1.1	142.5	1.8	40.6	2.7	145.4	19.7	3435	-	M	short
V0460	199.9	0.1	188.3	1.5	121.4	2.2	32.7	3.7	-	-	3435	-	M	short
V0461	400.1	0.01	41.2	0.2	74.3	0.4	35.5	4.5	18.5	1.2	3435	-	L	ok
V0462	400.1	0.01	37.8	0.2	61.4	0.3	31.7	2.9	-	-	3435	-	L	ok
V0463	400.1	0.01	40.6	0.2	72.6	0.5	35.9	4.4	-	-	3435	-	L	ok
V0464	400.1	0.02	61.1	0.4	84.0	0.7	36.7	3.1	-	-	3435	-	L	ok
V0465	400.1	0.02	63.8	0.4	94.0	0.8	40.9	2.4	-	-	3435	-	L	ok
V0466	400.1	0.02	62.7	0.5	90.3	0.6	38.2	2.6	30.6	3.2	3435	-	L	ok
V0467	400.1	0.03	80.5	0.8	96.6	0.8	37.0	2.7	-	-	3435	-	L	ok
V0468	400.1	0.03	81.2	0.7	98.4	0.8	38.7	3.2	42.7	0.3	3435	-	L	ok
V0469	400.1	0.03	82.9	0.6	108.1	0.7	42.5	2.4	-	-	3435	-	L	ok
V0470	400.1	0.04	98.6	1.0	109.0	1.3	38.2	3.2	-	-	3435	-	M	short
V0471	400.1	0.04	99.8	0.6	116.0	0.9	41.9	2.9	52.8	1.0	3435	-	M	ok
V0472	400.1	0.04	97.2	1.0	101.6	1.7	38.4	3.4	-	-	3435	-	M	short
V0473	500.0	0.01	42.2	0.6	76.6	0.6	37.7	3.2	-	-	3435	-	L	ok
V0474	500.0	0.01	44.3	0.7	83.6	0.7	39.1	3.6	19.2	5.2	3435	-	L	ok
V0475	500.0	0.01	43.2	0.6	81.2	0.7	37.6	2.4	-	-	3435	-	L	ok
V0476	500.0	0.02	64.0	0.9	91.6	0.9	38.4	2.6	-	-	3435	-	L	ok
V0477	500.0	0.02	66.0	0.6	101.1	0.8	42.3	2.5	-	-	3435	-	L	ok
V0478	500.0	0.02	65.6	0.6	98.7	1.0	39.9	2.3	54.9	31.8	3435	-	L	ok
V0479	500.0	0.1	234.1	14.0	603.5	23.7	39.9	2.3	86.4	50.6	3435	-	H	error
V0480	40.0	0.06	139.5	3.6	115.9	4.1	34.7	2.8	-	-	3348	-	L	ok
V0481	40.0	0.06	142.7	3.8	127.8	4.8	39.7	2.4	109.5	15.4	3348	-	L	ok
V0482	40.0	0.06	140.4	3.7	121.2	4.4	36.9	2.5	-	-	3348	-	L	ok
V0483	40.0	0.15	290.2	7.9	174.8	8.7	42.1	3.1	-	-	3348	-	M	ok

Test	$v_c$ [m/min]	$f$ [mm/rev]	$F_c$ [N]	$\sigma_{F_c}$ [N]	$F_f$ [N]	$\sigma_{F_f}$ [N]	$r_n$ [ $\mu$ m]	$\sigma_{r_n}$ [ $\mu$ m]	$h_{avg}$ [ $\mu$ m]	$\sigma_{h_{avg}}$ [ $\mu$ m]	$l_{cut}$ [mm]	$T_{chip}$ [K]	Wear	Status
V0484	40.0	0.15	286.8	7.5	173.3	10.3	40.0	3.4	177.7	-	3348	-	M	ok
V0485	40.0	0.15	285.3	7.4	162.7	9.8	38.0	2.4	-	-	3348	-	M	ok
V0486	40.0	0.2	349.7	6.5	178.7	9.7	33.2	4.4	-	-	3348	-	M	ok
V0487	40.0	0.2	352.3	5.2	169.1	6.0	33.4	3.1	-	-	3348	-	M	ok
V0488	40.0	0.2	353.1	6.2	180.6	8.8	37.2	3.3	233.7	-	3348	-	M	ok
V0489	125.0	0.06	141.9	2.2	123.3	2.0	37.7	3.2	-	-	3348	-	M	ok
V0490	125.0	0.06	141.7	2.3	122.8	2.3	37.9	3.3	88.5	8.6	3348	-	M	ok
V0491	125.0	0.06	141.9	2.2	125.2	2.1	39.0	3.2	98.9	16.1	3348	-	M	ok
V0492	125.0	0.15	258.3	2.6	150.5	1.8	37.1	4.0	-	-	3348	-	M	ok
V0493	125.0	0.15	256.5	2.6	137.3	1.7	34.6	3.2	-	-	3348	-	M	ok
V0494	125.0	0.15	259.2	2.6	154.2	1.9	39.3	2.7	171.6	2.7	3348	-	M	ok
V0495	125.0	0.2	322.3	4.9	166.6	5.0	35.4	2.4	-	-	3348	-	M	short
V0496	125.0	0.2	324.0	5.3	176.1	5.0	38.6	3.3	296.9	135.6	3348	-	M	short
V0497	125.0	0.2	321.7	4.1	173.4	3.6	42.9	4.6	-	-	3348	-	M	ok
V0498	100.0	0.06	143.9	3.1	136.8	3.7	46.8	2.8	-	-	3348	-	M	ok
V0499	100.0	0.06	142.5	3.4	132.2	4.0	40.5	3.2	147.5	51.8	3348	-	M	ok
V0500	100.0	0.06	140.9	3.1	128.7	3.6	39.3	3.0	-	-	3348	-	M	ok
V0501	100.0	0.12	229.3	2.0	147.5	1.4	39.1	3.0	156.1	4.4	3348	-	M	ok
V0502	100.0	0.12	227.1	1.9	142.5	1.6	37.7	2.9	-	-	3348	-	M	ok
V0503	100.0	0.12	229.4	1.9	149.9	1.6	38.1	2.9	-	-	3348	-	M	ok
V0504	100.0	0.2	325.2	4.1	172.5	2.3	39.4	4.0	-	-	3348	-	M	ok
V0505	100.0	0.2	329.4	4.1	177.2	2.7	41.0	2.2	241.5	2.0	3348	-	M	ok
V0506	100.0	0.2	323.9	3.8	164.0	2.4	35.9	2.7	-	-	3348	-	M	ok
V0507	150.0	0.06	138.2	1.4	118.3	1.1	36.5	3.0	-	-	3348	-	M	ok
V0508	150.0	0.06	139.8	1.4	130.6	1.5	41.0	2.8	109.3	21.5	3348	-	M	ok
V0509	150.0	0.06	137.4	1.3	117.1	1.2	37.3	3.0	-	-	3348	-	M	ok
V0510	150.0	0.12	218.6	1.7	144.3	1.7	39.0	2.4	149.9	13.8	3348	-	M	ok
V0511	150.0	0.12	219.6	1.8	149.3	1.9	41.2	2.3	-	-	3348	-	M	ok
V0512	150.0	0.12	216.9	1.7	137.5	1.5	35.4	2.2	-	-	3348	-	M	ok
V0513	150.0	0.2	324.2	4.7	176.0	7.3	36.0	2.9	-	-	3348	-	M	short
V0514	150.0	0.2	325.1	5.8	185.3	7.9	37.8	2.8	276.6	51.4	3348	-	M	short
V0515	150.0	0.2	326.2	5.2	184.0	7.3	37.3	2.1	-	-	3348	-	M	short
V0516	150.0	0.02	63.6	1.0	91.0	1.9	38.3	2.5	38.5	11.3	3348	-	L	ok
V0517	150.0	0.02	61.6	0.8	83.2	1.5	34.8	3.6	-	-	3348	-	L	ok
V0518	150.0	0.02	63.4	0.8	89.0	1.6	36.2	3.9	-	-	3348	-	L	ok
V0519	150.0	0.03	85.4	1.2	105.7	1.8	40.0	2.8	38.8	0.5	3348	-	L	ok
V0520	150.0	0.03	87.1	1.2	108.3	1.9	38.1	4.1	-	-	3348	-	L	ok

Table B.14: Experimental results Ti6Al4V orthogonal cutting tests

Test	$v_c$ [m/min]	$f$ [mm/rev]	$F_c$ [N]	$\sigma_{F_c}$ [N]	$F_f$ [N]	$\sigma_{F_f}$ [N]	$r_n$ [ $\mu$ m]	$\sigma_{r_n}$ [ $\mu$ m]	$h_{avg}$ [ $\mu$ m]	$\sigma_{h_{avg}}$ [ $\mu$ m]	$l_{cut}$ [mm]	$T_{chip}$ [K]	Wear	Status
V0069	10.1	0.01	52.1	11.0	31.6	6.7	33.9	1.6	-	-	6587	-	L	short
V0070	10.1	0.01	47.0	7.1	28.4	4.2	35.5	2.3	71.1	-	6587	360	L	ok
V0071	10.1	0.01	47.7	9.5	28.4	5.7	39.5	4.9	-	-	6587	-	L	ok
V0072	10.1	0.1	325.1	26.7	185.5	19.3	42.3	2.4	228.6	-	1317	360	L	ok
V0073	10.1	0.1	312.1	38.8	175.8	20.0	39.2	3.0	190.2	-	1317	360	L	ok
V0074	10.1	0.1	310.3	25.2	173.0	15.9	39.0	3.8	231.3	-	1317	360	L	ok
V0075	10.1	0.2	509.0	9.2	303.2	27.0	42.4	2.0	439.0	-	1317	360	L	saturation
V0076	10.1	0.2	543.9	39.7	306.9	30.7	39.2	4.0	367.9	-	1317	360	M	ok
V0077	10.1	0.2	543.7	39.9	298.6	32.0	42.4	2.3	516.4	-	1317	360	M	ok
V0078	10.1	0.2	542.9	32.6	297.3	28.2	33.2	4.7	444.3	-	1317	360	L	ok
V0079	70.1	0.01	38.5	9.5	24.3	6.4	41.2	2.5	69.0	-	4391	360	L	instable
V0080	70.1	0.01	38.0	9.0	23.7	5.6	36.3	4.6	-	-	6587	360	L	instable
V0081	70.1	0.01	37.0	9.8	23.3	6.2	42.4	2.5	90.4	-	21959	360	L	ok
V0082	70.1	0.1	283.7	14.6	233.6	25.6	40.6	2.6	-	-	1317	250	L	instable
V0083	70.1	0.1	329.6	8.9	319.8	11.2	39.5	3.6	-	-	1976	250	M	instable
V0084	70.1	0.1	379.7	4.0	401.0	5.7	38.2	4.1	395.5	-	4391	300	M	ok
V0085	70.1	0.1	387.3	2.9	412.2	2.9	43.8	2.3	414.8	4.3	4391	290	M	ok
V0086	70.1	0.2	612.8	9.9	511.3	2.7	38.1	3.5	-	-	2195	290	M	saturation
V0087	70.1	0.2	617.0	8.1	511.5	0.7	41.4	2.5	679.2	-	2195	290	M	saturation
V0088	70.1	0.2	614.7	8.5	511.5	0.7	41.4	2.5	606.5	-	2195	290	M	saturation
V0089	70.1	0.2	614.3	8.3	544.9	14.6	36.0	2.6	-	-	2195	290	M	instable
V0090	150.0	0.01	34.4	5.3	-169.7	4.0	39.8	2.5	57.7	14.2	21959	360	L	error
V0091	150.0	0.01	36.5	5.9	25.0	4.3	41.7	2.1	44.0	-	21959	360	L	ok
V0092	150.0	0.01	36.3	6.4	24.9	4.6	39.5	2.5	37.9	2.2	21959	360	L	ok
V0093	150.0	0.1	344.4	1.2	334.9	1.6	41.5	3.5	318.0	-	4391	290	M	ok
V0094	150.0	0.1	346.8	2.3	340.2	3.8	43.4	2.0	346.2	-	4391	290	M	ok
V0095	150.0	0.1	342.9	2.3	332.4	3.6	36.1	3.0	353.2	-	4391	290	M	ok
V0096	150.0	0.2	549.0	3.0	410.3	4.1	40.6	2.5	512.8	-	2195	290	M	ok
V0097	150.0	0.2	544.6	5.0	401.9	9.7	44.7	2.1	529.6	-	2195	360	M	ok
V0098	150.0	0.2	544.8	3.7	402.0	6.1	41.3	2.2	409.5	36.7	2195	340	M	ok
V0099	150.0	0.4	876.9	20.6	470.4	39.7	42.9	2.5	724.3	-	1097	320	M	instable
V0100	150.0	0.4	920.4	5.9	515.7	4.5	40.0	2.5	801.9	96.8	2195	340	M	ok
V0101	150.0	0.4	899.5	15.1	498.8	23.7	42.0	2.9	638.6	-	4940	340	M	ok
V0102	30.0	0.02	72.6	27.8	45.2	16.3	40.5	2.9	-	-	3440	360	L	ok
V0103	30.0	0.02	71.6	24.5	43.9	14.2	39.2	2.9	-	-	3440	360	L	ok
V0104	30.0	0.02	70.2	24.1	43.2	14.3	40.2	2.7	244.0	-	3440	360	L	ok
V0105	30.0	0.06	188.3	20.8	108.6	14.2	42.4	2.4	-	-	3440	360	L	questionable
V0106	30.0	0.06	170.6	29.0	96.9	16.4	36.0	3.9	108.3	-	3440	360	L	questionable
V0107	30.0	0.06	166.2	32.6	95.5	18.1	42.3	2.1	-	-	3440	360	L	questionable
V0108	30.0	0.15	377.0	29.3	216.1	19.9	38.3	2.9	242.4	-	3440	360	L	ok
V0109	30.0	0.15	370.1	27.3	209.4	20.3	42.9	2.3	257.9	-	3440	360	L	ok
V0110	30.0	0.15	377.1	26.8	218.9	18.8	39.9	2.7	221.5	22.9	3440	360	M	ok
V0111	100.0	0.02	64.0	18.6	41.2	12.1	40.5	2.4	-	-	3440	360	L	questionable
V0112	100.0	0.02	64.1	19.9	41.9	12.9	38.2	4.9	104.6	-	3440	360	L	questionable
V0113	100.0	0.02	63.2	12.6	41.2	8.3	42.4	3.0	48.4	-	3440	360	L	ok
V0114	100.0	0.06	198.4	2.9	177.9	4.6	41.6	2.3	-	-	3440	320	M	ok
V0115	100.0	0.06	196.9	2.3	175.5	3.9	38.1	4.5	-	-	3440	290	M	ok
V0116	100.0	0.06	195.8	2.7	172.6	4.8	37.3	3.7	161.5	-	3440	320	M	ok
V0117	100.0	0.15	455.2	6.2	405.4	12.7	38.4	3.5	506.9	21.2	3440	300	M	initially stable
V0118	100.0	0.15	461.8	6.5	420.1	11.5	37.2	4.0	-	-	3440	360	M	short
V0119	100.0	0.15	476.3	8.1	443.7	14.2	39.5	3.0	-	-	3440	360	M	initially stable
V0120	30.0	0.04	126.3	25.2	72.6	15.5	38.2	2.6	-	-	3440	360	L	questionable
V0121	30.0	0.04	127.7	23.3	75.3	13.3	40.5	3.1	117.7	14.8	3440	360	L	ok
V0122	30.0	0.04	121.7	35.2	71.5	20.1	35.2	4.5	-	-	3440	360	L	questionable

Test	$v_c$ [m/min]	$f$ [mm/rev]	$F_c$ [N]	$\sigma_{F_c}$ [N]	$F_f$ [N]	$\sigma_{F_f}$ [N]	$r_n$ [ $\mu$ m]	$\sigma_{r_n}$ [ $\mu$ m]	$h_{avg}$ [ $\mu$ m]	$\sigma_{h_{avg}}$ [ $\mu$ m]	$l_{cut}$ [mm]	$T_{chip}$ [K]	Wear	Status
V0123	30.0	0.1	262.5	23.4	152.9	15.5	43.1	2.1	-	-	3440	360	L	ok
V0124	30.0	0.1	253.2	26.7	144.5	16.8	39.0	2.9	-	-	3440	360	L	ok
V0125	30.0	0.1	258.1	25.7	147.2	15.7	38.4	2.5	147.3	-	3440	360	L	ok
V0126	30.0	0.2	488.6	26.6	289.1	23.2	39.6	3.2	-	-	3440	240	M	ok
V0127	30.0	0.2	501.3	28.5	307.1	30.0	44.0	2.1	448.1	78.9	3440	240	M	ok
V0128	30.0	0.2	493.3	25.7	296.3	25.5	40.6	3.5	-	-	3440	240	M	ok
V0129	100.0	0.04	122.9	8.3	91.6	9.0	43.4	2.1	109.1	15.7	3440	250	L	ok
V0130	100.0	0.04	120.1	10.7	85.4	8.7	31.6	3.3	-	-	3440	360	L	ok
V0131	100.0	0.04	113.6	12.7	79.9	11.4	36.5	4.7	-	-	3440	240	L	ok
V0132	100.0	0.1	350.9	3.1	360.2	5.4	39.2	3.5	-	-	3440	320	M	short
V0133	100.0	0.1	350.0	2.4	355.7	5.5	37.6	2.3	379.1	-	3440	320	M	short
V0134	100.0	0.1	353.6	1.8	364.8	2.8	38.3	2.7	-	-	3440	320	M	short
V0135	100.0	0.2	565.3	10.5	459.0	19.1	38.5	6.2	-	-	3440	340	M	initially stable
V0136	100.0	0.2	552.9	12.3	444.3	24.6	44.3	5.2	-	-	3440	320	M	initially stable
V0137	100.0	0.2	565.9	9.2	461.8	16.3	40.4	3.2	572.9	-	3440	340	M	initially stable
V0138	30.0	1.0	1590.6	61.8	1417.5	170.1	0.0	0.0	-	-	3440	-	H	saturation
V0139	50.1	0.02	67.9	25.9	41.2	15.0	38.9	3.7	145.6	-	3308	360	L	questionable
V0140	50.1	0.02	73.1	22.6	45.3	13.3	39.9	3.3	59.4	-	3308	360	L	questionable
V0141	50.1	0.02	68.0	28.1	42.1	17.0	40.4	2.6	-	-	3308	360	L	questionable
V0142	50.1	0.06	164.3	40.3	99.1	23.0	38.4	3.3	-	-	3308	360	L	ok
V0143	50.1	0.06	167.2	29.7	100.9	16.6	35.2	5.2	191.2	-	3308	360	L	ok
V0144	50.1	0.06	158.0	40.8	94.6	23.1	36.6	2.6	-	-	3308	360	L	ok
V0145	50.1	0.15	506.7	10.7	487.4	16.5	42.8	2.6	-	-	3308	240	M	short
V0146	50.1	0.15	511.1	6.1	493.2	9.5	43.3	2.5	614.2	-	3308	280	M	ok
V0147	50.1	0.15	504.7	7.7	483.2	15.1	38.1	2.8	-	-	3308	300	M	short
V0148	150.0	0.02	73.5	4.9	59.7	4.3	36.3	2.6	-	-	3308	260	L	ok
V0149	150.0	0.02	68.2	7.9	51.6	6.2	39.3	2.9	-	-	3308	360	L	ok
V0150	150.0	0.02	69.2	6.3	53.7	5.5	41.0	4.3	64.3	2.0	3308	240	L	ok
V0151	150.0	0.06	224.4	1.8	239.6	3.0	37.2	2.1	211.7	-	3308	340	M	ok
V0152	150.0	0.06	226.2	1.4	244.7	2.0	38.2	3.3	-	-	3308	340	M	ok
V0153	150.0	0.06	224.5	1.4	239.9	3.0	40.8	1.9	-	-	3308	340	M	initially stable
V0154	150.0	0.15	428.6	2.9	353.1	4.1	35.3	2.9	303.8	-	3308	340	M	ok
V0155	150.0	0.15	425.4	2.3	345.2	3.0	35.4	7.9	-	-	3308	340	M	ok
V0156	150.0	0.15	430.4	3.6	356.7	4.7	37.9	2.4	-	-	3308	300	M	ok
V0157	50.1	0.04	113.1	28.8	65.8	16.2	38.2	2.6	-	-	3308	360	L	questionable
V0158	50.1	0.04	122.7	23.1	73.0	13.4	37.8	4.4	114.1	22.1	3308	360	L	questionable
V0159	50.1	0.04	114.3	40.4	68.6	23.4	43.5	4.8	-	-	3308	360	L	questionable
V0160	50.1	0.1	262.1	19.9	168.6	18.4	42.2	3.0	-	-	3308	240	M	ok
V0161	50.1	0.1	261.7	20.0	167.3	17.0	39.5	2.0	-	-	3308	240	M	ok
V0162	50.1	0.1	257.4	18.4	160.1	14.1	33.6	3.0	253.0	-	3308	240	M	ok
V0163	50.1	0.2	654.4	6.4	623.0	10.6	42.4	2.4	-	-	3308	290	M	short
V0164	50.1	0.2	651.7	5.2	615.7	8.6	43.2	2.2	720.5	-	3308	340	M	short
V0165	50.1	0.2	649.6	5.3	613.7	8.6	42.1	2.9	520.6	-	3308	340	M	short
V0166	150.0	0.04	141.8	5.2	131.9	11.9	33.6	3.1	-	-	3308	300	M	initially stable
V0167	150.0	0.04	137.9	3.7	128.9	10.2	40.4	2.1	121.3	-	3308	340	M	initially stable
V0168	150.0	0.04	139.7	5.7	133.5	14.6	40.5	1.8	170.1	-	3308	320	M	initially stable
V0169	150.0	0.1	325.3	3.9	312.0	6.1	35.4	2.9	234.0	-	3308	340	M	short
V0170	150.0	0.1	322.4	6.1	307.5	10.7	36.3	2.7	-	-	3308	300	M	short
V0171	150.0	0.1	326.6	6.6	313.6	11.5	40.5	2.7	351.0	-	3308	340	M	short
V0172	150.0	0.2	517.5	7.9	373.6	13.5	32.7	3.6	-	-	3308	340	M	ok
V0173	150.0	0.2	519.2	4.3	377.3	5.5	40.3	4.5	406.8	-	3308	340	M	ok
V0174	150.0	0.2	520.0	12.2	380.3	20.9	40.7	2.8	410.9	-	3308	320	M	ok
V0175	150.0	0.02	77.3	3.7	77.2	1.7	36.0	3.0	80.3	5.6	165404	-	M	ok
V0176	10.0	0.02	80.9	15.4	48.6	8.9	39.0	2.4	46.8	-	3256	360	L	ok
V0177	10.0	0.02	81.9	16.3	49.3	9.5	40.6	2.8	74.4	-	3256	360	L	ok
V0178	10.0	0.02	80.8	16.4	48.3	9.2	37.2	2.7	-	-	3256	360	L	ok
V0179	10.0	0.06	195.0	29.5	111.5	15.5	43.5	1.8	241.6	-	3256	360	L	ok
V0180	10.0	0.06	190.9	18.7	106.3	10.8	33.9	2.7	-	-	3256	360	L	ok
V0181	10.0	0.06	189.1	28.3	104.9	15.4	35.1	3.4	-	-	3256	360	L	ok
V0182	10.0	0.15	404.7	24.7	221.7	18.4	41.3	2.2	-	-	3256	360	L	ok
V0183	10.0	0.15	409.8	22.6	225.3	18.9	35.8	2.4	-	-	3256	360	L	ok
V0184	10.0	0.15	414.3	23.3	233.3	19.9	40.3	2.0	272.5	21.5	3256	360	L	ok
V0185	69.9	0.02	62.9	7.8	36.8	5.1	30.0	3.5	-	-	3256	360	L	ok
V0186	69.9	0.02	66.1	22.0	40.6	13.8	36.4	2.5	68.7	12.3	3256	360	L	ok
V0187	69.9	0.02	66.7	12.3	40.9	7.6	40.9	2.3	-	-	3256	360	L	ok
V0188	69.9	0.06	167.1	17.3	109.0	12.7	37.5	4.8	-	-	3256	360	M	ok
V0189	69.9	0.06	167.0	16.7	109.4	11.7	39.9	2.8	150.3	22.4	3256	360	M	ok
V0190	69.9	0.06	166.2	15.1	107.8	10.7	36.1	3.5	-	-	3256	360	M	ok
V0191	69.9	0.15	501.5	5.3	491.3	7.8	39.3	2.8	463.7	-	3256	300	M	short
V0192	69.9	0.15	497.3	3.7	485.0	6.1	32.9	4.6	-	-	3256	300	M	short
V0193	69.9	0.15	501.2	3.6	490.2	6.3	39.5	3.2	-	-	3256	300	M	short
V0194	199.9	0.01	36.9	3.3	26.0	2.5	33.5	3.2	27.2	4.7	3256	360	L	ok
V0195	199.9	0.01	39.5	3.8	28.3	2.9	40.5	3.8	-	-	3256	360	L	ok
V0196	199.9	0.01	39.5	3.2	28.4	2.8	39.5	3.1	-	-	3256	360	L	ok
V0197	199.9	0.04	159.1	1.0	171.3	1.6	40.8	3.1	-	-	3256	290	M	ok
V0198	199.9	0.04	158.0	1.2	170.2	1.8	33.0	4.1	166.2	-	3256	290	M	ok
V0199	199.9	0.04	159.3	0.9	172.3	1.1	38.3	3.7	-	-	3256	290	M	ok
V0200	199.9	0.08	269.7	2.8	261.2	4.1	41.6	4.0	260.9	4.4	3256	360	M	short
V0201	199.9	0.08	268.2	2.5	257.7	3.5	36.3	3.6	287.7	-	3256	360	M	short
V0202	199.9	0.08	273.3	2.6	267.9	4.2	40.9	2.8	-	-	3256	360	M	short
V0203	300.0	0.01	49.6	0.9	51.7	1.2	35.8	3.4	-	-	3256	290	M	ok
V0204	300.0	0.01	51.5	1.2	55.9	1.8	38.6	2.7	47.7	3.3	3256	360	M	ok
V0205	300.0	0.01	51.2	1.2	55.6	1.7	37.8	3.0	52.7	3.2	3256	360	M	ok
V0206	300.0	0.04	146.9	3.3	150.4	3.4	43.5	2.0	-	-	3256	360	M	short
V0207	300.0	0.04	149.2	3.2	152.9	5.3	41.7	2.5	134.6	-	3256	360	M	short
V0208	300.0	0.04	149.9	2.4	152.9	3.5	36.6	2.9	-	-	3256	360	M	short
V0209	300.0	0.08	260.1	2.7	233.5	1.9	42.4	3.0	-	-	3256	360	M	short
V0210	300.0	0.08	259.7	1.4	233.0	1.0	43.3	2.5	246.9	-	3256	360	M	short
V0211	300.0	0.08	257.5	1.8	227.2	2.1	40.4	2.3	-	-	3256	360	M	short
V0212	10.0	0.01	45.2	14.2	28.6	8.3	36.9	2.9	-	-	3256	360	L	ok
V0213	10.0	0.01	46.0	7.4	28.7	4.6	40.5	2.6	31.2	12.2	3256	360	L	ok
V0214	10.0	0.01	44.9	7.8	27.6	4.6	35.4	2.8	-	-	3256	360	L	ok
V0215	10.0	0.04	144.6	27.7	84.1	16.0	39.1	2.9	86.8	16.5	3256	360	L	ok
V0216	10.0	0.04	145.4	27.6	85.1	15.2	41.6	3.4	-	-	3256	360	L	ok
V0217	10.0	0.04	138.0	30.8	79.1	16.8	39.6	2.8	-	-	3256	360	L	ok
V0218	10.0	0.08	249.5	20.2	142.7	12.1	36.3							

Test	$v_c$ [m/min]	$f$ [mm/rev]	$F_c$ [N]	$\sigma_{F_c}$ [N]	$F_f$ [N]	$\sigma_{F_f}$ [N]	$r_n$ [ $\mu$ m]	$\sigma_{r_n}$ [ $\mu$ m]	$h_{avg}$ [ $\mu$ m]	$\sigma_{h_{avg}}$ [ $\mu$ m]	$l_{cut}$ [mm]	$T_{chip}$ [K]	Wear	Status
V0222	349.9	0.01	56.3	0.5	61.1	0.4	42.6	2.0	-	-	3256	360	L	ok
V0223	349.9	0.01	54.0	0.5	56.0	0.4	39.8	1.9	36.5	3.8	3256	360	L	ok
V0224	349.9	0.04	152.1	1.1	156.1	1.6	36.2	2.5	-	-	3256	360	M	short
V0225	349.9	0.04	152.1	0.8	154.1	1.5	34.9	2.2	143.2	-	3256	360	M	short
V0226	349.9	0.04	153.4	2.0	158.2	2.7	38.7	3.1	-	-	3256	360	M	short
V0227	349.9	0.08	250.3	2.3	213.0	2.1	40.6	2.6	-	-	3256	360	M	short
V0228	349.9	0.08	245.8	2.0	203.6	2.3	36.5	2.2	216.3	-	3256	360	M	short
V0229	349.9	0.08	242.0	3.0	198.0	2.8	34.6	3.2	-	-	3256	360	M	short
V0230	250.1	0.02	83.6	0.5	82.3	0.4	43.0	1.8	-	-	3256	320	M	ok
V0231	250.1	0.02	81.6	0.5	79.3	0.5	39.8	2.5	64.0	5.4	3256	300	M	ok
V0232	250.1	0.02	82.5	0.7	80.6	0.5	41.6	3.0	-	-	3256	300	M	ok
V0233	250.1	0.06	207.7	2.4	202.2	3.9	39.9	3.5	-	-	3256	360	M	short
V0234	250.1	0.06	213.0	2.8	212.8	4.1	41.3	2.4	192.1	7.5	3256	360	M	short
V0235	250.1	0.06	206.2	2.3	198.2	3.8	33.3	3.7	-	-	3256	360	M	short
V0236	250.1	0.1	304.0	1.8	256.9	2.8	38.6	2.2	312.8	-	3256	360	M	ok
V0237	250.1	0.1	304.5	2.8	258.5	4.0	39.5	2.3	-	-	3256	360	M	short
V0238	250.1	0.1	304.6	2.6	258.2	3.2	39.2	2.8	-	-	3256	360	M	short
V0239	349.9	0.02	87.8	0.7	93.5	0.9	36.2	2.5	91.4	19.6	3256	360	M	short
V0240	349.9	0.02	88.7	0.9	94.4	1.0	33.6	2.9	-	-	3256	360	M	short
V0241	349.9	0.02	89.3	1.3	97.2	1.6	35.2	3.0	-	-	3256	360	M	short
V0242	349.9	0.06	207.1	2.1	194.6	2.5	38.2	3.4	-	-	3256	360	M	short
V0243	349.9	0.06	208.6	2.4	199.6	3.0	39.7	2.4	-	-	3256	360	M	short
V0244	349.9	0.06	204.3	2.2	187.9	3.0	34.7	3.0	215.3	-	3256	360	M	short
V0245	349.9	0.1	285.0	2.6	216.7	1.8	40.1	2.5	263.8	-	3256	360	M	ok
V0246	349.9	0.1	283.0	3.5	212.8	5.4	37.7	2.6	-	-	3256	360	M	ok
V0247	349.9	0.1	283.3	3.1	215.1	3.8	39.5	2.7	-	-	3256	360	M	ok
V0248	349.9	0.15	-0.0	0.1	-0.0	0.1	33.6	2.8	-	-	3256	360	M	error
V0249	349.9	0.15	369.7	4.8	229.6	6.0	35.2	3.1	346.4	-	3256	360	M	ok
V0250	349.9	0.15	375.2	3.3	236.9	4.2	38.4	3.0	-	-	3256	360	M	ok
V0251	499.9	0.02	-0.0	0.1	-0.0	0.1	40.3	2.3	58.0	0.4	3256	360	M	error
V0252	50.0	0.01	39.7	13.2	26.8	7.9	34.3	3.8	-	-	3260	360	L	ok
V0253	50.0	0.01	38.0	9.0	24.2	5.6	40.0	2.4	69.3	13.2	3260	360	L	ok
V0254	50.0	0.01	37.8	7.4	24.4	4.7	40.4	3.3	-	-	3260	360	L	ok
V0255	50.0	0.08	211.2	24.2	128.1	15.2	36.0	2.8	168.3	21.5	3260	360	M	ok
V0256	50.0	0.08	210.5	26.3	128.9	16.8	38.3	2.1	152.9	-	3260	360	L	ok
V0257	50.0	0.08	209.5	29.4	128.9	18.0	38.1	2.3	-	-	3260	360	M	ok
V0258	50.0	0.12	320.4	19.8	234.3	33.8	40.2	2.3	-	-	3260	200	M	short
V0259	50.0	0.12	325.1	16.7	241.1	29.7	41.2	2.5	339.0	-	3260	200	M	short
V0260	50.0	0.12	322.7	20.0	238.8	36.0	40.5	2.0	-	-	3260	200	M	short
V0261	250.0	0.01	51.1	0.5	53.9	0.7	35.6	3.1	35.2	-	3260	300	L	ok
V0262	250.0	0.01	52.6	1.1	57.3	1.3	41.6	2.1	-	-	3260	300	L	short
V0263	250.0	0.01	49.3	0.9	51.4	1.3	35.5	2.9	-	-	3260	300	L	short
V0264	250.0	0.08	250.4	1.8	223.6	2.6	32.0	3.1	-	-	3260	360	M	short
V0265	250.0	0.08	255.7	2.7	234.4	3.4	37.0	2.1	-	-	3260	360	M	short
V0266	250.0	0.08	259.8	2.9	241.9	3.9	40.6	2.4	249.9	-	3260	360	M	short
V0267	250.0	0.12	335.9	2.9	265.3	3.3	41.7	2.2	-	-	3260	360	M	ok
V0268	250.0	0.12	330.6	1.5	253.5	1.8	33.3	3.2	-	-	3260	360	M	ok
V0269	250.0	0.12	334.6	1.8	262.0	2.2	38.3	2.8	336.2	-	3260	360	M	ok
V0270	50.0	0.18	0.0	0.0	0.0	0.0	38.0	2.3	-	-	2173	360	M	ok
V0271	50.0	0.18	566.4	8.5	521.5	9.9	36.6	2.6	404.6	29.5	2173	360	M	ok
V0272	50.0	0.18	569.1	8.6	527.6	12.9	38.7	2.7	-	-	2173	360	M	ok
V0273	50.0	0.18	572.7	8.9	536.3	13.1	36.0	2.9	-	-	2173	360	M	ok
V0274	50.0	0.22	678.0	7.3	614.7	12.0	38.5	2.4	-	-	2173	360	M	ok
V0275	50.0	0.22	678.0	9.8	615.2	12.3	37.6	2.5	683.3	-	2173	360	M	ok
V0276	50.0	0.22	679.5	13.3	612.1	24.7	40.1	1.9	-	-	2173	360	M	short
V0277	200.0	0.02	84.4	1.8	83.5	2.3	38.2	2.3	-	-	3260	300	M	questionable
V0278	200.0	0.02	81.1	1.1	80.3	1.1	40.1	2.6	70.0	6.6	3260	300	M	ok
V0279	200.0	0.02	79.8	1.0	77.9	1.3	36.2	3.6	-	-	3260	300	M	ok
V0280	200.0	0.06	213.6	1.9	220.6	3.3	38.8	2.6	198.3	6.5	3260	360	M	short
V0281	200.0	0.06	213.1	1.4	218.9	2.4	38.9	2.3	-	-	3260	360	M	short
V0282	200.0	0.06	215.6	1.4	224.1	2.6	38.8	3.0	-	-	3260	360	M	short
V0283	200.0	0.1	307.6	2.5	275.4	4.3	35.9	2.8	-	-	3260	360	M	short
V0284	200.0	0.1	308.3	2.3	272.1	3.6	37.1	3.6	-	-	3260	360	M	short
V0285	200.0	0.1	310.3	3.0	279.7	4.3	37.9	2.3	325.5	88.9	3260	360	M	short
V0286	450.0	0.02	86.5	1.2	91.1	0.6	40.0	2.7	65.4	7.7	3260	360	M	short
V0287	450.0	0.02	86.5	1.2	92.9	0.9	41.1	2.3	-	-	3260	360	M	short
V0288	450.0	0.02	86.2	1.5	92.9	1.6	40.6	2.3	-	-	3260	360	M	short
V0289	450.0	0.06	193.1	2.6	167.8	1.9	38.0	2.4	142.9	2.5	3260	360	M	short
V0290	450.0	0.06	196.0	3.6	173.7	2.1	40.3	2.2	-	-	3260	360	M	short
V0291	450.0	0.06	190.1	2.1	162.1	1.8	34.4	3.6	-	-	3260	360	M	short
V0292	450.0	0.1	265.1	3.2	183.9	2.9	41.8	2.1	-	-	3260	300	M	ok
V0293	450.0	0.1	263.6	2.2	180.2	1.2	37.5	2.8	237.7	-	3260	300	M	ok
V0294	450.0	0.1	261.6	3.6	178.5	3.8	37.4	2.1	-	-	3260	300	M	ok
V0295	50.0	0.2	644.5	4.6	611.4	6.9	34.3	3.5	-	-	3260	360	M	ok
V0296	50.0	0.2	643.6	4.6	608.4	6.1	37.7	2.7	503.9	-	3260	360	M	ok
V0297	50.0	0.2	642.6	14.5	596.9	23.9	38.3	2.5	-	-	3260	360	M	ok
V0298	500.0	0.1	259.6	1.9	169.5	2.6	37.2	3.8	-	-	3260	280	M	ok
V0299	500.0	0.1	259.4	2.5	173.2	3.6	40.2	3.4	240.7	-	3260	280	M	ok
V0300	500.0	0.1	260.3	1.5	174.6	2.3	42.0	2.4	228.2	8.4	3260	280	M	ok

Table B.15: Experimental results Ck45 orthogonal cutting tests

## Appendix C. Kienzle Parameters

The Kienzle coefficients are given as a function of cutting speed for Ti6Al4V in table C.16 and for Ck45 in C.17.

$v_c$	[m/min]	11	13	20	40	50	52	60	70	74	80	89	100	125	150	159	162	191	212	254	318	381	400	500
$k_{c1.1}$	[N/mm <sup>2</sup> ]	1299	1264	1265	1253	1061	1156	1146	1156	941	1084	891	932	962	998	869	1027	881	859	749	712	663	803	662
$m_c$	[-]	0.21	0.22	0.22	0.22	0.28	0.27	0.27	0.24	0.32	0.28	0.34	0.33	0.31	0.3	0.31	0.28	0.32	0.32	0.37	0.36	0.38	0.35	0.41
$k_{f1.1}$	[N/mm <sup>2</sup> ]	413	333	421	352	274	328	300	282	282	267	177	226	283	283	235	303	255	248	199	186	205	329	280
$m_f$	[-]	0.51	0.63	0.54	0.61	0.7	0.66	0.69	0.69	0.69	0.73	0.89	0.77	0.69	0.7	0.72	0.67	0.71	0.72	0.8	0.78	0.75	0.66	0.73

Table C.16: Ti6Al4V: Kienzle coefficients for feed and cutting force estimations.

$v_c$	[m/min]	10	30	50	70	100	150	200	250	300	350	450
$k_{c1.1}$	[N/mm <sup>2</sup> ]	1935	1803	1417	1729	1672	1707	1716	1794	1851	1575	1368
$m_c$	[-]	0.19	0.17	0.51	0.35	0.32	0.28	0.26	0.22	0.22	0.27	0.29
$k_{f1.1}$	[N/mm <sup>2</sup> ]	996	995	654	1156	809	765	1030	1268	1446	1024	587
$m_f$	[-]	0.23	0.2	0.96	0.55	0.65	0.6	0.45	0.31	0.29	0.38	0.53

Table C.17: Ck45: Kienzle coefficients for feed and cutting force estimations.

## References

- [1] Paul Albrecht. New developments in the theory of the metal-cutting process: part i. the ploughing process in metal cutting. 1960.
- [2] PJ Arrazola, T Özel, D Umbrello, M Davies, and IS Jawahir. Recent advances in modelling of metal machining processes. *CIRP Annals-Manufacturing Technology*, 62(2):695–718, 2013.
- [3] Bijish Babu and Lars-Erik Lindgren. Dislocation density based model for plastic deformation and globularization of ti-6al-4v. *International Journal of Plasticity*, 50:94–108, 2013.
- [4] Thomas HC Childs. Revisiting flow stress modelling for simulating chip formation of carbon and low alloy steels. *Procedia CIRP*, 82:26–31, 2019.
- [5] Ashwin Devotta, Tomas Beno, Ronnie Löf, and Emil Espes. Quantitative characterization of chip morphology using computed tomography in orthogonal turning process. *Procedia CIRP*, 33:299–304, 2015.
- [6] ENISO DIN. 25178-606, 2013-12. *Geometrische Produktspezifikation (GPS)–Oberflächenbeschaffenheit: Flächenhaft–Teil*, 606.
- [7] ENISO DIN. 6892-1: Metallische werkstoffe-zugversuch-teil 1: Prüfverfahren bei raumtemperatur. *Deutsches Institut für Normung: Berlin, Germany*, 2009.
- [8] DIN50125:2016-12. Prüfung metallischer werkstoffe – zugproben, December 2016.
- [9] F Ducobu, E Rivière-Lorphèvre, and E Filippi. Experimental contribution to the study of the ti6al4v chip formation in orthogonal cutting on a milling machine. *International Journal of Material Forming*, 8(3):455–468, 2015.
- [10] F Ducobu, E Rivière-Lorphèvre, and E Filippi. On the importance of the choice of the parameters of the johnson-cook constitutive model and their influence on the results of a ti6al4v orthogonal cutting model. *International Journal of Mechanical Sciences*, 122:143–155, 2017.
- [11] Ralf Förster and Anna Förster. Werkstoffe. In *Einführung in die Fertigungstechnik*, pages 137–164. Springer, 2018.

- [12] Francis H Froes and Ma Qian. *Titanium in medical and dental applications*. Woodhead Publishing, 2018.
- [13] M Hardt, D Schraknepper, and T Bergs. Investigations on the application of the downhill-simplex-algorithm to the inverse determination of material model parameters for fe-machining simulations. *Simulation Modelling Practice and Theory*, 107:102214, 2021.
- [14] Mikko Hokka, Jari Rämö, Ahmad Mardoukhi, Taina Vuoristo, Armin Roth, and V-T Kuokkala. Effects of microstructure on the dynamic strain aging in ferritic-pearlitic steels. *Journal of Dynamic Behavior of Materials*, 4(4):452–463, 2018.
- [15] SI Jaffery and PT Mativenga. Assessment of the machinability of ti-6al-4v alloy using the wear map approach. *The International Journal of Advanced Manufacturing Technology*, 40(7):687–696, 2009.
- [16] GR Johnson and WH Cook. A constitutive modeling and data for metals subjected to large strain rates and high temperatures. *Proceedings of 7th international symposium on ballistics*, pages 541–577, 1983.
- [17] Jaydeep Karandikar, Anirban Chaudhuri, Timothy No, Scott Smith, and Tony Schmitz. Bayesian optimization for inverse calibration of expensive computer models: a case study for johnson-cook model in machining. *Manufacturing Letters*, 2022.
- [18] Otto Kienzle. Die bestimmung von kräften und leistungen an spanenden werkzeugen und werkzeugmaschinen. *VDI-Z*, 94(11):299–305, 1952.
- [19] Hagen Klippel. *Constitutive Equations for Simulation of Metal Cutting with Meshless Methods on GPU*. PhD thesis, ETH Zurich, 2021.
- [20] Hagen Klippel, Marcel Gerstgrasser, Darko Smolenicki, Ezio Cadoni, Hans Roelofs, and Konrad Wegener. Johnson cook flow stress parameter for free cutting steel 50sib8. *arXiv preprint arXiv:2007.14087*, 2020.
- [21] Fritz Klocke. Schneidkantenpräparation. In *Fertigungsverfahren 1*, pages 229–249. Springer, 2018.
- [22] Wilfried König. *Fertigungsverfahren 1: Drehen, Fräsen, Bohren*. Springer-Verlag, 2008.
- [23] Linus Meier. Methods to reduce variation in cutting tool life tests. *The International Journal of Advanced Manufacturing Technology*, 103(1):355–365, 2019.
- [24] Linus Meier, Nikolas Schaal, and Konrad Wegener. In-process measurement of the coefficient of friction on titanium. *Procedia Cirp*, 58:163–168, 2017.
- [25] M Eugene Merchant. Mechanics of the metal cutting process. i. orthogonal cutting and a type 2 chip. *Journal of applied physics*, 16(5):267–275, 1945.
- [26] M Eugene Merchant. Mechanics of the metal cutting process. ii. plasticity conditions in orthogonal cutting. *Journal of applied physics*, 16(6):318–324, 1945.
- [27] Ashwin Moris Devotta, PV Sivaprasad, Tomas Beno, and Mahdi Eynian. Predicting continuous chip to segmented chip transition in orthogonal cutting of c45e steel through damage modeling. *Metals*, 10(4):519, 2020.

- [28] Otai. Otai homepage. <https://www.otaisteel.com/products/carbon-steel/din-c45e-steel-ck45-carbon-structural-steel-din-17200-en10083/>, 2022. Accessed: 28.03.2022.
- [29] Manfred Peters and Christoph Leyens. *Titan und titanlegierungen*. Wiley-VCH Weinheim, 2002.
- [30] Manfred Peters, Jörg Kumpfert, Charles H Ward, and Christoph Leyens. Titanium alloys for aerospace applications. *Advanced engineering materials*, 5(6):419–427, 2003.
- [31] Alokesh Pramanik and Guy Littlefair. Machining of titanium alloy (ti-6al-4v)—theory to application. *Machining science and technology*, 19(1):1–49, 2015.
- [32] Sandvik. Sandvik homepage. [https://www.sandvik.coromant.com/de-de/products/Pages/productdetails.aspx?c=CCMW%2009%20T3%2004%20%20%20%20%20H13A](https://www.sandvik.coromant.com/de-de/products/Pages/productdetails.aspx?c=CCMW%2009%20T3%2004%20%20%20%20%20%20H13A), 2021. Accessed: 23.02.2021.
- [33] Abraham Savitzky and Marcel JE Golay. Smoothing and differentiation of data by simplified least squares procedures. *Analytical chemistry*, 36(8):1627–1639, 1964.
- [34] ASTM Standard. E8/e8m-13a. *Standard Test Methods for Tension Testing of Metallic Materials*, ASTM International, West Conshohocken, PA, 2013.
- [35] Benedikt Thimm. *Werkstoffmodellierung und Kennwertermittlung für die Simulation spanabhebender Fertigungsprozesse*. PhD thesis, Universität Siegen, 2018.
- [36] CA Van Luttervelt, THC Childs, IS Jawahir, F Klocke, PK Venuvinod, Y Altintas, E Armarego, D Dornfeld, I Grabec, J Leopold, et al. Present situation and future trends in modelling of machining operations progress report of the cirp working group ‘modelling of machining operations’. *CIRP Annals*, 47(2):587–626, 1998.
- [37] Pauli Virtanen, Ralf Gommers, Travis E. Oliphant, Matt Haberland, Tyler Reddy, David Cournapeau, Evgeni Burovski, Pearu Peterson, Warren Weckesser, Jonathan Bright, Stéfan J. van der Walt, Matthew Brett, Joshua Wilson, K. Jarrod Millman, Nikolay Mayorov, Andrew R. J. Nelson, Eric Jones, Robert Kern, Eric Larson, C J Carey, İlhan Polat, Yu Feng, Eric W. Moore, Jake VanderPlas, Denis Laxalde, Josef Perktold, Robert Cimrman, Ian Henriksen, E. A. Quintero, Charles R. Harris, Anne M. Archibald, Antônio H. Ribeiro, Fabian Pedregosa, Paul van Mulbregt, and SciPy 1.0 Contributors. SciPy 1.0: Fundamental Algorithms for Scientific Computing in Python. *Nature Methods*, 17:261–272, 2020. doi: 10.1038/s41592-019-0686-2.
- [38] C-F Wyen and Konrad Wegener. Influence of cutting edge radius on cutting forces in machining titanium. *CIRP annals*, 59(1):93–96, 2010.
- [39] Carl-Frederik Wyen. *Rounded cutting edges and their influence in machining titanium*. PhD thesis, ETH Zürich, 2011.
- [40] Carl-Frederik Wyen, Wolfgang Knapp, and Konrad Wegener. A new method for the characterisation of rounded cutting edges. *The International Journal of Advanced Manufacturing Technology*, 59(9-12):899–914, 2012.
- [41] Muhammad Younas, Syed Husain Imran Jaffery, Ashfaq Khan, and Mushtaq Khan. Development and analysis of tool wear and energy consumption maps for turning of titanium alloy (ti6al4v). *Journal of Manufacturing Processes*, 62:613–622, 2021.